

SIMULATION OF THE EFFECTS OF ACOUSTIC NOISE ON MEMS GYROSCOPES

Except where reference is made to the work of others, the work described in this thesis is my own or was done in collaboration with my advisory committee. This thesis does not include proprietary or classified information.

Grant Roth

Certificate of Approval:

Dan Marghitu
Professor
Mechanical Engineering

George T. Flowers, Chair
Professor
Mechanical Engineering

Robert Dean
Assistant Professor
Electrical and Computer Engineering

George T. Flowers
Dean
Graduate School

SIMULATION OF THE EFFECTS OF ACOUSTIC NOISE ON MEMS GYROSCOPES

Grant Roth

A Thesis

Submitted to

the Graduate Faculty of

Auburn University

in Partial Fulfillment of the

Requirements for the

Degree of

Master of Science

Auburn, Alabama
August 10, 2009

SIMULATION OF THE EFFECTS OF ACOUSTIC NOISE ON MEMS GYROSCOPES

Grant Roth

Permission is granted to Auburn University to make copies of this thesis at its discretion, upon the request of individuals or institutions and at their expense. The author reserves all publication rights.

Signature of Author

Date of Graduation

VITA

Grant Roth, son of James and Rebecca Roth, was born on August 17, 1983, in Huntsville, AL. In 2001 he began attending Auburn University where he received his Bachelors of Software Engineering in 2005. He then enrolled in the Mechanical Engineering Masters program at Auburn University in 2006.

THESIS ABSTRACT

SIMULATION OF THE EFFECTS OF ACOUSTIC NOISE ON MEMS GYROSCOPES

Grant Roth

Master of Science, August 10, 2009
(B.S., Auburn University, 2005)

120 Typed Pages

Directed by George T. Flowers

Recent advances in MEMS technology have resulted in relatively low cost gyroscopes and accelerometers. The low cost of these devices has led to inexpensive inertial measurement systems, opening up a wide variety of possible applications for inertial measurement units (IMUs) with environmental conditions ranging from mild to harsh. This study focuses on MEMS gyroscopes, which are based upon vibratory, rather than rotational designs, that have been proven susceptible to the effects of acoustic noise. In some aerospace environments this is particularly true. In these environments the noise levels can reach higher than 120 dB with frequencies reaching in excess of 20kHz. These effects can overwhelm the output signals causing them to become extremely contaminated and even completely saturated. A model is developed to simulate testing the gyroscope exposed to high frequency noise. The model also simulates the use of several types of acoustic foams to mitigate the effect of high frequency noise. The model simulates high frequency noise as high frequency vibration. Samples of the foams will be tested to determine their ability to mitigate simulated high frequency noise. The information gathered from these tests will be used in the model to mitigate the effects of the high frequency acoustic

noise simulated by use of high frequency vibration applied to the gyroscope in the model. Following testing with the model, several ADXRS300 gyroscopes were tested in an acoustically harsh environment to determine the effects of the high frequency acoustic noise. The foams were also tested to provide data to validate the model.

ACKNOWLEDGMENTS

The author would like to thank Dr. George T. Flowers for his encouragement, guidance, and invaluable help at every stage of this work. The author also wishes to acknowledge Dr. Robert Dean and Dr. Dan Marghitu for their evaluation and advice with this work. The author would also like to express his gratitude to Simon Castro for help during the course of testing. The author would also like to thank his friends and family for their continued support during this effort.

Style manual or journal used Journal of Approximation Theory (together with the style known as “aums”). Bibliography follows van Leunen’s *A Handbook for Scholars*.

Computer software used The document preparation package T_EX (specifically L^AT_EX) together with the departmental style-file `aums.sty`.

TABLE OF CONTENTS

LIST OF TABLES	xi
LIST OF FIGURES	xii
1 INTRODUCTION	1
1.1 Motivations & Objectives	1
1.2 Review of Previous Works	2
1.3 Organization of this Thesis	4
2 BACKGROUND	5
2.1 History	5
2.2 Background	5
2.3 Applications	8
2.4 Acoustic Noise	8
3 SIMULATION	10
3.1 Modeling of Gyroscope Dynamics	10
3.2 Model Results	11
4 EXPERIMENTAL SETUP	18
4.1 Experimental Test Setup	18
4.2 Test Results	20
4.2.1 Baseline Testing	20
4.2.2 Foam Testing	23
5 CONCLUSION	73
BIBLIOGRAPHY	75
APPENDICES	77
A DERIVATION OF EQUATIONS OF MOTION	78

B	SIMULATION CODE	80
B.1	Plotting	80
B.2	Initialization Data	87
B.2.1	init_Data.m	87
B.2.2	init_Data2.m	89
B.2.3	init_Data3.m	90
B.3	Files That Run ode45	91
B.3.1	sim_run.m	91
B.3.2	sim_run2.m	94
B.3.3	sim_run3.m	97
B.4	Equations of Motion	100
B.4.1	sim_try.m	100
B.4.2	sim_try2.m	103
B.4.3	sim_try3.m	105

LIST OF TABLES

3.1	Initial data for simulations	11
3.2	Simulations performed	12
4.1	List of resonant frequencies of gyroscopes	21
4.2	Sound levels	23
4.3	The absolute difference in output voltage between baseline of no noise to that of noise during tests with foams for the reference gyro	24

LIST OF FIGURES

2.1	Simple vibratory gyroscope	6
3.1	Simulation results without noise and for 130dB with 0dB, 8dB, 10dB, and 15dB of isolation with noise	13
3.2	Comparison of simulation output without noise and with 130dB of simulated noise	14
3.3	Comparison of simulation output for tests at 130dB without isolation and with 8dB of isolation	15
3.4	Comparison of simulation output for tests at 130dB without isolation and with 10dB of isolation	16
3.5	Comparison of simulation output for tests at 130dB without isolation and with 15dB of isolation	17
4.1	Gyroscopes mounted to the rate table	25
4.2	Gyroscope mounting plate	25
4.3	Basic configuration of the test setup	26
4.4	Control area directly external to the acoustic chamber	27
4.5	Block diagram of configuration for monitoring sound levels	28
4.6	Reference gyro frequency sweep from 6kHz to 18kHz	28
4.7	Output response from the reference gyroscope at resonant frequency of 13907.77Hz	29
4.8	Output response from gyro 2 at resonant frequency	30
4.9	Output response from gyro 3 at resonant frequency	31

4.10	Output response from gyro 4 at resonant frequency	32
4.11	Output response from gyro 5 at resonant frequency	33
4.12	Output response from gyro 7 at resonant frequency	34
4.13	Output response from gyro 8 at resonant frequency	35
4.14	Output response from gyro 9 at resonant frequency	36
4.15	Output response from gyro 12 at resonant frequency	37
4.16	Output response from gyro 12 at resonant frequency with y-scale enlarged	38
4.17	Output response from gyro 13 at resonant frequency	39
4.18	Output response from gyro 13 at resonant frequency with y-scale enlarged	40
4.19	Output response from gyro 14 at resonant frequency	41
4.20	Output response from gyro 15 at resonant frequency	42
4.21	Output response from gyro 15 at resonant frequency with y-scale enlarged	43
4.22	Output response from gyro 16 at resonant frequency	44
4.23	Output response from gyro 18 at resonant frequency	45
4.24	Output response from gyro 19 at resonant frequency	46
4.25	Output response from gyro 19 at resonant frequency with y-scale enlarged	47
4.26	Output response from gyro 20 at resonant frequency	48
4.27	Output response from gyro 20 at resonant frequency with y-scale enlarged	49
4.28	Output response from gyro 21 at resonant frequency	50
4.29	Output response from gyro 21 at resonant frequency with y-scale enlarged	51

4.30	Output response from gyro 22 at resonant frequency	52
4.31	Output response from gyro 23 at resonant frequency	53
4.32	Output response from gyro 23 at resonant frequency with y-scale enlarged	54
4.33	Output response from gyro 24 at resonant frequency	55
4.34	Photograph of foam samples used during the experimental testing . .	56
4.35	Output responses from the reference gyro without foam and with gray foam	57
4.36	Output responses from the reference gyro without foam and with black foam	58
4.37	Output responses from the reference gyro without foam and with pink foam	59
4.38	Output responses from the reference gyro without foam and with blue foam	60
4.39	Output responses from the reference gyro without foam and with green foam	61
4.40	A comparison of the reference gyro's output signal for all foams . . .	62
4.41	Output responses from gyro 14 without foam and with gray foam . .	63
4.42	Output responses from gyro 14 without foam and with black foam . .	64
4.43	Output responses from gyro 14 without foam and with pink foam . .	65
4.44	Output responses from gyro 14 without foam and with blue foam . .	66
4.45	Output responses from gyro 14 without foam and with green foam . .	67
4.46	Output responses from gyro 16 without foam and with gray foam . .	68
4.47	Output responses from gyro 16 without foam and with black foam . .	69
4.48	Output responses from gyro 16 without foam and with pink foam . .	70
4.49	Output responses from gyro 16 without foam and with blue foam . .	71
4.50	Output responses from gyro 16 without foam and with green foam . .	72

CHAPTER 1

INTRODUCTION

Microelectromechanical systems (MEMS) are devices within the scale of 1mm to $1\mu\text{m}$ that combine electrical components with mechanical systems [1]. The small size of MEMS devices has opened up a wide variety of applications to sensing technology that had been previously limited due to size constraints. The MEMS gyroscopes in this study have recently become more widely used due to this reduction in size and the decrease in manufacturing costs. Applications for MEMS transducers in general have environments that range from completely benign to extremely harsh. Examples of harsh environments include high frequency vibration, extreme temperatures, mechanical shock, and high frequency, high power acoustic noise. Recent studies have focused on the effects of high frequency vibration, extreme temperatures and mechanical shock on such devices. Little research has been performed in the area of high frequency acoustic noise. This work is an investigation into mitigation techniques, with the objective of providing the ground work for further research in the field and further development of noise mitigation techniques for the MEMS gyroscope.

1.1 Motivations & Objectives

This thesis is the result of a desire to investigate what effects high frequency, high power acoustic noise can have on MEMS gyroscopes, and the attempt to mitigate the adverse effects caused by such noise. This is not meant to be an exhaustive

search of mitigation techniques, but rather a focused study of one particular device using specific mitigation strategies.

The major objectives are:

- To demonstrate that high frequency, high power acoustic noise has an effect on a MEMS gyroscope
- To develop a model of a MEMS gyroscope exposed to high frequency, high power acoustic noise
- To examine strategies for isolating this model from simulated high frequency, high power acoustic noise
- To experimentally validate mitigation techniques of the effects of the acoustic noise on the MEMS gyroscope.

1.2 Review of Previous Works

A review of previous research in the field of high frequency, high power acoustic noise on gyroscopes yielded few results. This section will provide an overview and summary of what was found and other similar studies in MEMS applications.

Weinberg [2] discussed potential error sources in vibratory tuning fork gyroscopes. The error sources discussed in this paper focus mainly on design aspects. Weinberg presented the following reasons for vacuum packaging: it reduces the required driving force of the device; it increases bandwidth of the device; the resolution is enhanced due to lower damping; and it reduces the hydrodynamic lift. As an error source, Weinberg also cited mechanical quadrature caused by imperfections in the manufacturing process and electrical coupling of capacitance which causes false output signals. Saukoski discussed sources of zero-rate output errors identifying these

sources as manufacturing defects, interface electronics, environmental vibration and temperature. The article includes several methods of compensating for quadrature error, as well as methods for distinguishing the sources[13].

Pryputniewicz used an optoelectronic laser interferometric microscope to compare thermal expansion of attachment methods such as gold bump, gold/tin braze, and mechanical interposer. The deformation of each method was measured at different temperatures. This research indicated that the mechanical interposer produced the least deformation at higher temperatures of all attachment methods examined in the study. During the course of this research, it was also discovered that the anchors connecting the proof mass to the frame could have deformations of up to 40nm dependent on the fabrication process[3].

Dean, et al. proved that vibration at or near the resonant frequency of a MEMS gyroscope has an adverse effect on the output signal. It was also proven that these effects can be mitigated by integrating a low-pass filter into the die level packaging, by suspending the article between two membranes of rubbery or soft material, and by creating a low-pass filter in printed circuit board laminate[6]. This research was extended in another study using electrostatic actuators to create an active filter, allowing the filters to have a variable damping coefficient and spring constant. These active filters provided increased performance over the passive filters in the mitigation of vibration[7].

Another study by Dean proved that wide-band high power acoustic noise can have an effect on MEMS gyroscopes. This study used four commercially available gyroscopes, the ADXRS300, the SiRRS01, the QDARS and the Tokin gyroscope. At noise levels approaching 100dB, it was seen that the gyroscope's noise floors were increasing, and at levels near 130dB, the gyroscopes yielded no reliably usable

data[4]. In a continuation of the study by Dean, Castro subjected an inertial measurement unit containing multiple MEMS gyroscopes to the same wind tunnel noise used in the previous study[5]. The inertial measurement unit was isolated from the noise by surrounding it with different types and thicknesses of foams. The foams provided sufficient isolation to prevent complete corruption of the output data.

1.3 Organization of this Thesis

This thesis is organized as follows:

Chapter 2 contains background information of gyroscopes including MEMS gyroscopes. Chapter 3 describes the development of a simulation of MEMS gyroscopes and the simulation results. Chapter 4 discusses the experimental test procedures and results. Chapter 5 summarizes the results and discusses the observations and conclusions of this research.

CHAPTER 2

BACKGROUND

This chapter provides a brief description of the function of traditional gyroscopes. It also provides a description of MEMS gyroscopes and applications for which these sensors are best suited.

2.1 History

The inertial gyroscope dates back to the early 1800's. Over the years, there have been a number of major advances in gyroscope technology. Until the development of MEMS devices, there were two major types of conventional gyroscopes- mechanical and optical. Traditional mechanical gyroscopes incorporate a spinning rotor free to rotate about a spin axis which is contained within a frame called a gimbal that is allowed to freely move in one or two axes[8]. Traditional optical gyroscopes utilize the Sagnac effect using two beams of laser generated light traveling in two different directions through a ring of optical fiber; the rate of rotation is calculated by the determining the distance the light has traveled[8]. The optical types of gyroscopes are not as affected by harsh environments as are mechanical gyroscopes on the other hand; optical gyroscopes are not as compact as MEMS gyroscopes.

2.2 Background

MEMS gyroscopes are fabricated using micromachining techniques. For those interested in specific details, an excellent discussion and overview is provided in

Chapters 15-23 of *The MEMS Handbook*[1]. MEMS gyroscopes do not rely on a spinning rotor as used in conventional mechanical gyroscopes because fabricating rotating parts with significant useful mass is difficult at the micro level[10]. Instead, a mechanical member is driven to resonance in one axis which excites a secondary vibration in the same structure or a vibration in secondary structure, due to the Coriolis effect[9].

Figure 2.1 shows a basic diagram of a vibratory gyroscope.

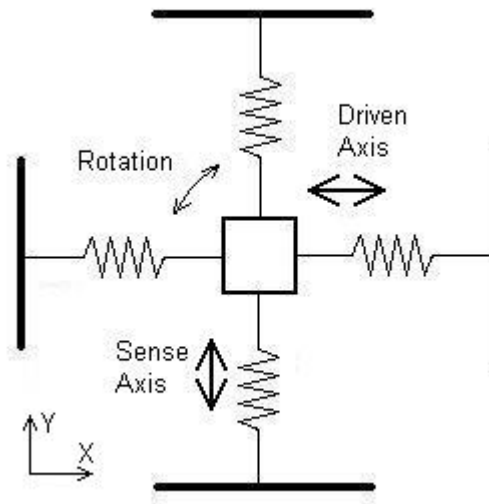


Figure 2.1: Simple vibratory gyroscope

The Coriolis acceleration and Coriolis force are defined as:

$$\vec{a}_c = 2\vec{\Omega} \times \vec{v}_r \quad (2.1)$$

$$\vec{F}_c = 2m\vec{\Omega} \times \vec{v}_r \quad (2.2)$$

The particular gyroscope design that is the focus of this research is a tuning fork vibratory gyroscope and uses a combdrive to drive the proof mass to resonance, resulting in a Coriolis coupling between the two degrees of freedom. The basic

equations of motion for a vibratory gyroscope are similar to that of a spring mass damper system. The derivation of the following equations of motion is shown in Appendix A.

$$m\ddot{x} + c_x\dot{x} + (k_x - m\dot{\Theta}^2)x - 2m\dot{\Theta}\dot{y} - m\ddot{\Theta}y = F_d \quad (2.3)$$

$$m\ddot{y} + c_y\dot{y} + (k_y - m\dot{\Theta}^2)y + 2m\dot{\Theta}\dot{x} + m\ddot{\Theta}x = 0 \quad (2.4)$$

$$m\ddot{\Theta}(x^2 + y^2 + \frac{1}{12}(l_x^2 + l_y^2)) + 2m\dot{\Theta}(x\dot{x} + y\dot{y}) - m\dot{y}\ddot{x} + m\dot{x}\ddot{y} = 0 \quad (2.5)$$

where m is the mass, k_x, k_y, c_x , and c_y are defined as follows, Q is the quality factor, ω_d is the drive axis resonant frequency, and ω_s is the resonant frequency of the sense axis:

$$k_x = \omega_d^2 m \quad (2.6)$$

$$k_y = \omega_s^2 m \quad (2.7)$$

$$c_x = \frac{m\omega_d}{Q} \quad (2.8)$$

$$c_y = \frac{m\omega_s}{Q} \quad (2.9)$$

while F_d is defined as:

$$F_d = \frac{2.28N\epsilon TV_{dc}V_{ac}\sin\omega_{drive}t}{g_c} \quad (2.10)$$

Here N is the number of capacitors created by fingers in the combdrive, ϵ is the dielectric constant, T is the thickness, V_{dc} and V_{ac} are the driving voltages, and g_c is the gap between the fingers in the combdrive[11].

2.3 Applications

Traditional gyroscopes have limitations in some of the applications where the future use of IMUs is concerned. These applications are better suited for IMUs based on MEMS technology. There have been considerable advancements in micromachined mechanical transducers in recent years, which have allowed the size, power requirements, and production cost of these devices to decrease. Low production costs, power requirements, and small size have allowed the introduction of MEMS transducers into a variety of new applications. Examples of these applications are consumer products such as videogames and cell phones, automotive stability control and rollover sensors, and small aerospace vehicles. These transducers are exposed to a variety of environments depending on their application. These environments range from benign to severe, where severe applications have harsh characteristics that can have an adverse effect on the ability of these devices to perform properly. Recently, research has focused on MEMS gyroscopes and the effects caused by mechanical shock, high frequency vibrations, and extreme temperatures. With the use of MEMS gyroscopes in both aerospace and commercial applications, it is not difficult to identify environments that contain high power, high frequency acoustic noise. This high power, high frequency acoustic noise can have detrimental effects on the output of these devices.

2.4 Acoustic Noise

The average person's hearing range is approximately 20Hz - 20kHz. The level of noise present in certain environments can be as high as or higher than 150dB. Examples of the dB scale of acoustic noise are as follows: 30dB would be the average noise level in a quiet place such as a library; 60dB is the average conversation; 90dB

would be traffic near an interstate highway; 110dB is the output of pneumatic tools; 120dB is considered to be painful without the use of hearing protection; 150dB and higher cause immediate hearing loss.[12] The gyroscopes used in this study were found to be effected at levels around 100dB [5]. The effects of high frequency acoustic noise can be transmitted to the device through contact between the package of the device and through the fluid surrounding the device similar to the manner in which the effects of high frequency vibration are transmitted to the device through the chassis. If the acoustic energy frequency components are close to the natural frequency of the mechanical structure in the MEMS gyroscope, it can produce undesirable motion of the sensor proof mass resulting in a corruption of the output signal.

CHAPTER 3

SIMULATION

This chapter describes the simulation model development and the simulation results.

3.1 Modeling of Gyroscope Dynamics

As described in Chapter 2, recall the equations 2.3, 2.4, 2.5, and 2.10. These are the equations of motion for a tuning fork gyroscope. The simulation consists of several MATLAB files, with one containing the equations of motion for the gyroscope with an additional noise term. The equation used to simulate the acoustic noise as a vibration is shown in 3.1.

$$F_{noise} = n \sin \omega_{sense} t \quad (3.1)$$

This simulated noise term is introduced into the x and y equations of motion. The level of noise, n , is calculated before it is introduced to the equations of motion, using a method to acquire the correct values to provide similar results to that of the physical gyroscope. The equation follows where *sound_level* is equivalent to the sound level in the chamber reduced by 100 and *noise_isolation* is equivalent to insertion loss of the simulated acoustic foams.

$$n = .75(\textit{sound_level} - \textit{noise_isolation}) \quad (3.2)$$

The frequency of the vibration is equivalent to that of the sense direction resonant frequency with some of the simulations performed with the frequency above and below this value. The output of the simulation is converted into a voltage based on calculations performed on a sample ADXRS300, as shown in Equation 3.3.

$$V_{out} = \frac{3}{400} \left(\frac{180}{\Pi} \dot{\Theta} \right) + 2.5 \quad (3.3)$$

The MATLAB run files documented in Appendix B run MATLAB function ode45 in three phases. In the first and third phases, the amplitude is reduced to zero, while in the second phase the amplitude is varied for each test run.

3.2 Model Results

Using the initial values found in Table 3.1, the model was simulated several times with differences due only to the adjustment in the amount of simulated Noise Reduction. The test results are presented in Figures 3.1-3.5. These simulations were performed with no simulated rotation of the device to be similar to the tests conducted on the experimental subjects.

Variable	Value
Timestep	0.1s
SPL	130dB
Freq	14000Hz
Rotation	0 deg/s

Table 3.1: Initial data for simulations

Test	Noise	Noise Reduction
No Noise	0dB	0dB
No Isolation	130dB	0dB
8dB Isolation	130dB	8dB
10dB Isolation	130dB	10dB
15dB Isolation	130dB	15dB

Table 3.2: Simulations performed

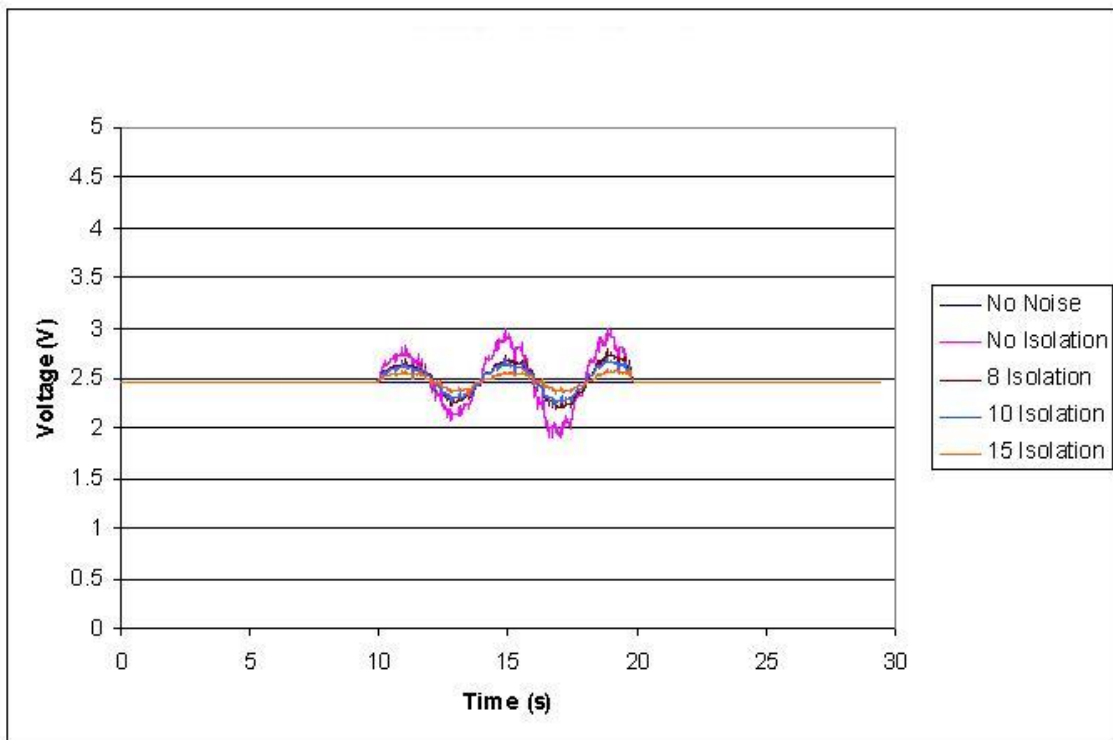


Figure 3.1: Simulation results without noise and for 130dB with 0dB, 8dB, 10dB, and 15dB of isolation with noise

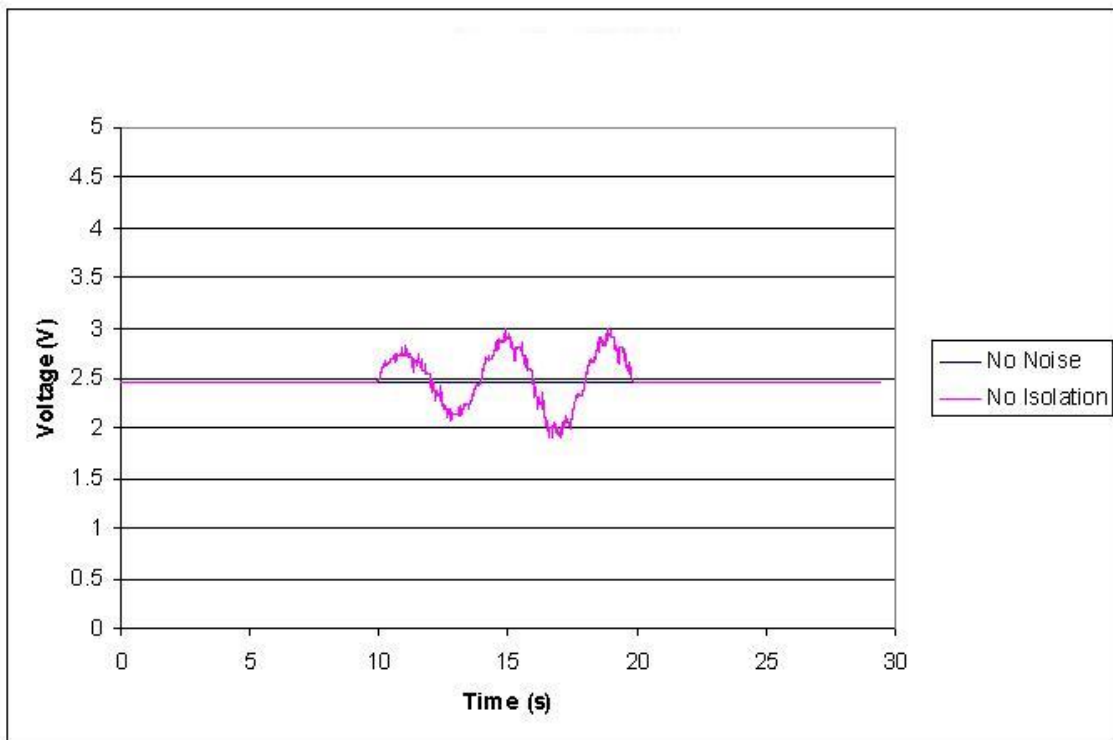


Figure 3.2: Comparison of simulation output without noise and with 130dB of simulated noise

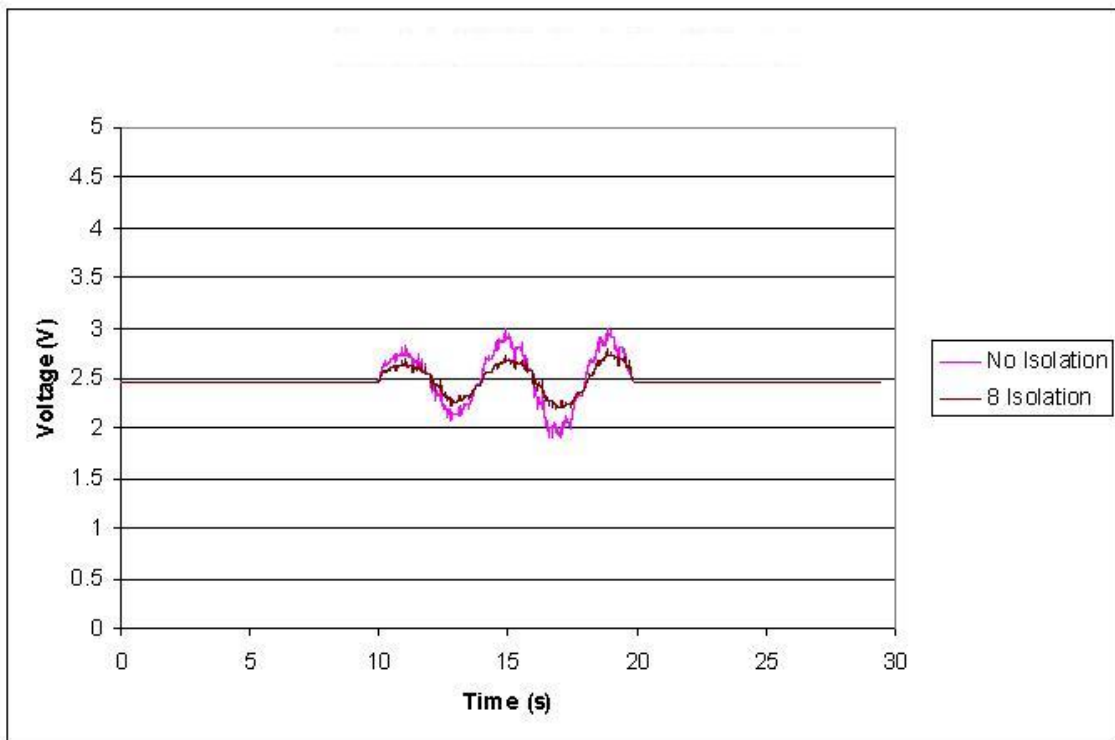


Figure 3.3: Comparison of simulation output for tests at 130dB without isolation and with 8dB of isolation

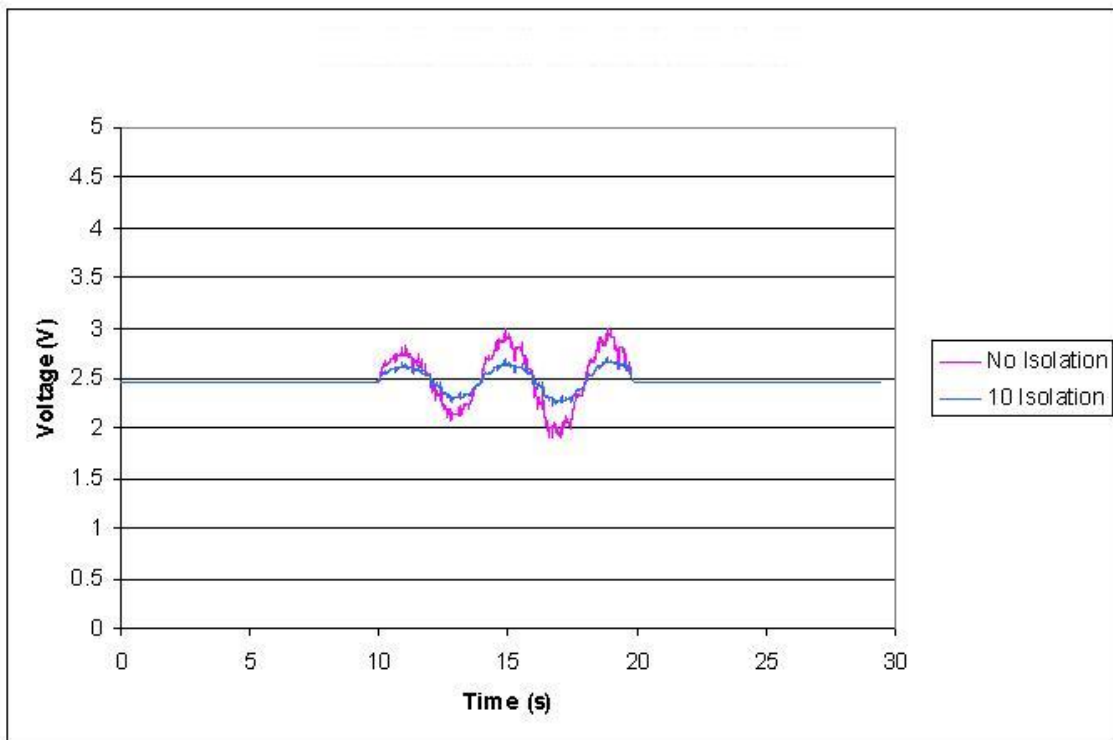


Figure 3.4: Comparison of simulation output for tests at 130dB without isolation and with 10dB of isolation

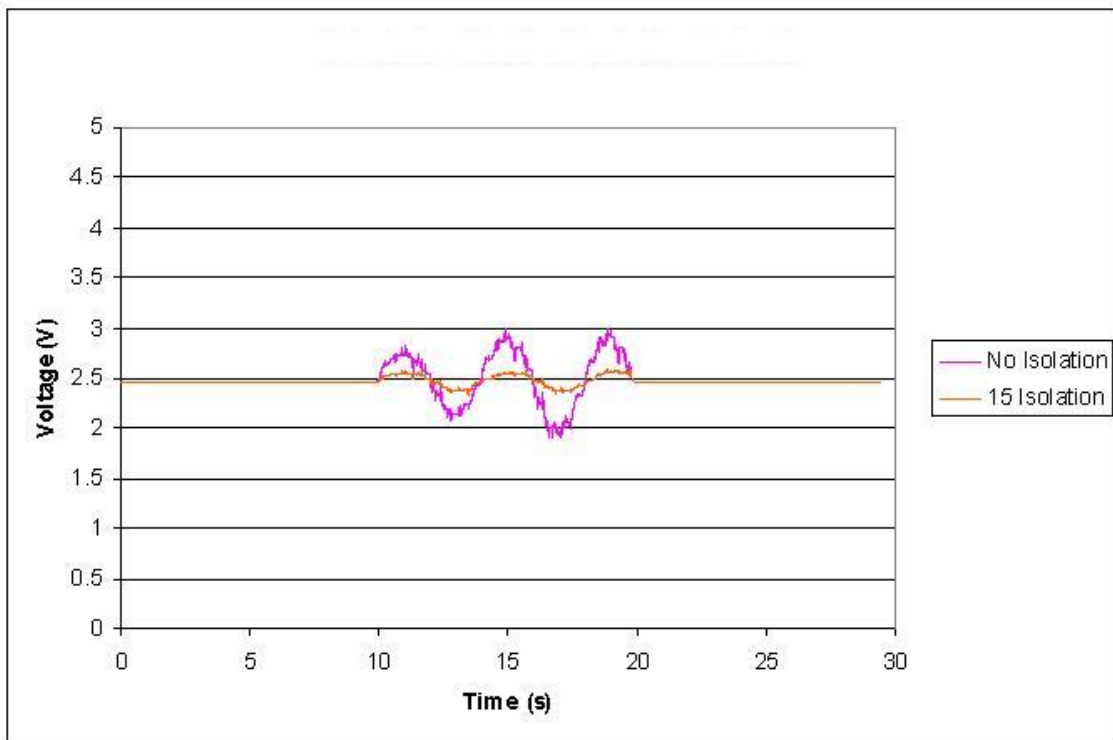


Figure 3.5: Comparison of simulation output for tests at 130dB without isolation and with 15dB of isolation

CHAPTER 4

EXPERIMENTAL SETUP

This chapter describes the experimental test setup and discusses the tests and test procedures.

4.1 Experimental Test Setup

The experimental tests were performed within an acoustic isolation chamber. The experimental configuration inside the chamber included a computer controlled single axis rate table from Aerotech. This rate table was attached to a massive aluminum base plate to prevent the device from rocking. In order to attach the gyroscopes to the table, a plate was designed and machined to allow the wires to have access to the mounting points that correspond to the individual gyroscope boards. This plate is adequate for mounting up to 5 individual gyroscope circuit boards, as seen in Figure 4.1. Figure 4.2 is a diagram of the plate (with the dimensions removed which allows the mounting positions to be observed).

The rate table was surrounded by a frame which supported several acoustic drivers. The two drivers that provided the high frequency noise are Community Speakers VHF-100 drivers. These drivers are capable of outputs of up to 140dB at frequencies higher than 12kHz. Additional high range acoustic noise was provided by an EV DH1A all purpose driver. The other two drivers in this experimental configuration are also made by Community Speakers. They are a M4 for the low range frequencies and an EM282 for the middle range. The frame provided adjustment of

the high and midrange speakers and held the low range speaker directly over the rate table. Figure 4.3 shows the basic layout of the test setup inside the acoustic chamber. The control area for the experiments was external to the acoustic chamber, as shown in Figure 4.4. The control area consisted of two computers, each containing a data acquisition card. The primary computer was responsible for generating the noise and recording the output from the gyroscopes. This computer provided the control for the rate table. The secondary computer was used only for monitoring and recording sound output levels via the piezo-electric microphone located inside the chamber. National Instruments Labview software was used to create virtual instrumentation to provide recordings of the data from both the gyroscopes and the microphone. The block diagram of this is shown in Figure 4.5. NCH Software's Tone Generator was used to create the high frequency noise used in these experiments. This software has the ability to create multiple tones, sweeps over ranges of tones, and several types of noise generation, while allowing control over the dB level created in the software. The tones generated by the software were then passed through the computer's sound card into two Crown XTi-1000 model amplifiers. The ability of the computer tone generating software to control the sound output level to the amplifiers simplified some tests by allowing more precise control over the pressure level in the chamber rather than controlling the analog inputs for output power level on the amplifiers. A script was written using AutoHotKey to make testing more efficient and to create less potential for human error.

4.2 Test Results

4.2.1 Baseline Testing

The MEMS gyroscopes used during the experiments are model ADXRS300 from Analog Devices. Testing began with one gyroscope used as the reference. First, the device was subjected to high frequency sound sweeps between 6kHz and 18kHz to determine the frequency that had the most detrimental effect on the output signal. A sample is shown in Figure 4.6. The high frequency sound sweep range was narrowed after calculating which frequencies were closest from visual inspection of the output signal. After narrowing the sweep to what was perceived to be the correct frequency, the tests were changed from continuous noise to 30 second tests with no sound for 10 seconds, followed by 10 seconds of sound, and completed with 10 seconds of silence. This format was used throughout the remaining tests. When the resonant frequency of the device was found, errors were generated in the device's output signal as shown in Figure 4.7. After it was shown that high power acoustic noise had such a detrimental effect, the other gyros were tested to see if they were responsive to such effects. Figures 4.8-4.33 show the output of the gyros during these tests. It was found that the frequency of noise for the reference gyroscope was different from the rest of the gyroscopes tested. Table 4.1 shows the different resonant frequencies for each of the gyroscopes.

The output for Gyro 2 in Figure 4.8 demonstrates the drastic effect on the output signal due to the exposure to high power noise. The signal spikes downward to about 1.75V then promptly rises to almost 3.5V remaining at that level until the noise is removed. The output signal from this device during noise exposure is similar to that of a gyroscope rotating at an approximate rate of 120deg/s. Examining the output of Gyro 3 in Figure 4.9 reveals an immediate drop due to the introduction

Gyro Number	Frequency (Hz)
Reference (1)	13903.77
2	15386
3	16234
4	16340
5	15796
7	14255
8	16071
9	13836
12	15433.51
13	15576
14	15689.6
15	16009.62
16	15983.83
18	13766
19	13640.75
20	14041
21	15923.59
22	15732
23	15943.1
24	15933.5

Table 4.1: List of resonant frequencies of gyroscopes

of the high power noise. This noise creates a false output signal at just below 2V, which would be the equivalent of a rotation at 60deg/s. The output from Gyro 4 in Figure 4.10 is similar to that of Gyro 3 but the signal has a sinusoidal pattern during exposure to the noise. This can cause detrimental effect on a system as it is generating output signals similar to a Gyroscope that has a varying rotational rate. The effects had on the output signal from Gyro 5 can be seen in Figure 4.11. The signal quickly spikes down to under 1.75V and then climbs back to 3.25V.

Gyro 6 was non-functional during testing. Figure 4.12 shows a downward spike followed by an gradual increase to the baseline voltage followed by a small spike when the acoustic noise was removed from the environment. As shown in Figure 4.13 Gyro 8 experienced a drop in voltage as the noise was introduced. However,

as the noise continued the signal began to take on a sinusoidal pattern. Figure 4.14 shows the response of Gyro 9 to its resonant frequency having a sharp drop under 2V then immediate spike to almost 4V followed by a leveling off at 3V. This would be similar to a rapid change from no rotation to -60 deg/s then to 180 deg/s and changing to 60 deg/s.

Gyro 10 was also non-functional for the tests performed. Gyro 11 was non-functional through out the testing process. Gyro 12 in Figure 4.15 presents an increase in the noise floor that can be seen in Figure 4.16. The detail in Figure 4.17 seems to not show change in output signal for Gyro 13. However in Figure 4.18 it also shows an increase in voltage and an increase in the noise in the output signal.

Figure 4.19 shows an almost sinusoidal output signal that swings from -60 deg/s to almost 60 deg/s. Gyro 15 in Figure 4.20 demonstrates a minute reaction to the noise similar to those of Gyro 12 and Gyro 13. Figure 4.21 reveals that Gyro 15 has a small increase in voltage that gradually begins to decrease until the removal of the noise. Gyro 16 in Figure 4.22 reveals reactions similar to that of Gyro 14; however, the voltage swing is much less than that of Gyro 14. Gyro 17 was non-functional throughout testing.

In Figure 4.23 Gyro 18 demonstrates a sudden drop off followed by erratic output signal changes until the removal of noise. Figures 4.24-4.25 show the output of Gyro 19. Figure 4.25 displays the details of an increase of voltage followed by sinusoidal drop and peak before the noise is removed. Gyro 20 shows a initial spike followed by a drop in voltage as seen in Figure 4.27. Gyro 21 in Figure 4.29 experiences a drop followed by a half sinusoidal motion that is not perceived in Figure 4.28.

Figure 4.30 shows that Gyro 22 has inverted reaction to the noise that is similar to that of Gyro 5. Gyro 23 in Figure 4.32 demonstrates a small voltage change that

begins to drop through the duration of the noise portion of the test. The output of Gyro 24 in Figure 4.33 shows a voltage drop while exposed to the high frequency noise. While each gyro was affected by the acoustic noise it was determined that the effects of the acoustic noise did not have an established pattern.

4.2.2 Foam Testing

Several different types of foams were used in the testing - a half inch thick gray closed cell foam, half inch thick black closed cell foam, and three different types of open cell foam (pink, blue, and green) which were all 1 inch thick. The black and gray foams were doubled in thickness for the tests to create one inch cubes of foam. The insertion loss for each of these foams is listed in Table 4.2. These tests were performed by inserting the microphone into the foam and measuring the sound level recorded. This shows that the black foam has an advantage at reducing the amount of noise in the baseline measured tests with the microphone.

Foam	Sound Level (dB)
No Foam	130
Gray	122
Black	119
Pink	120
Blue	122
Green	121

Table 4.2: Sound levels

The tests consisted of placing the shaped foam over the gyroscope then subjecting the device again to its resonant frequency in order to determine what effect the foam had as a mitigation technique. Figures 4.35-4.39 present a comparison of the effects of the noise with and without each type of foam on the reference gyroscope. The average increase in output voltage due to the noise over the baselines at the

beginning and end of each test, where there was no noise for each type of foam, can be seen in Table 4.3.

Foam	Absolute Difference (V)
Gray	0.010681
Black	0.005188
Pink	0.006256
Blue	0.011750
Green	0.005646

Table 4.3: The absolute difference in output voltage between baseline of no noise to that of noise during tests with foams for the reference gyro

This shows that the black foam was the most effective at mitigating the effects of the noise for the reference gyro, as indicated by the smallest average voltage change. Figure 4.40 shows a comparison of the mitigation effects of the foams. During testing of the mitigation techniques, several of the gyroscopes began to perform sporadically, perhaps due to the exposure to extended periods of high power, high frequency noise. There were only two other gyroscopes that would perform reliably during the testing. These gyroscopes were numbers 14 and 16. A comparison of the effects of noise with and without each type of foam on Gyro 14 is seen in Figures 4.41-4.45. The data provided from Gyro 14 generated inconclusive results as the foams appear to have had no effect on mitigating the acoustic noise at its respective resonant frequency. Gyro 16, however, as shown in Figures 4.46-4.50, provided useful data with the black foam having the greatest effect at reducing the effects of noise in Gyro 16. The results of these tests seem to indicate that the black foam has a better overall ability to mitigate the effects. The results from Gyro 16 also confirm that the black foam has the highest noise reduction of all the foams. This seemed to be predicted as the insertion loss of the black foam was greater than that of the rest of the other types of foam.



Figure 4.1: Gyroscopes mounted to the rate table

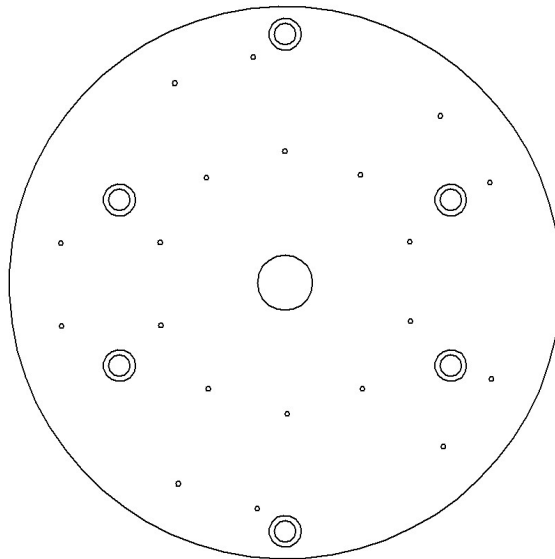


Figure 4.2: Gyroscope mounting plate



Figure 4.3: Basic configuration of the test setup



Figure 4.4: Control area directly external to the acoustic chamber

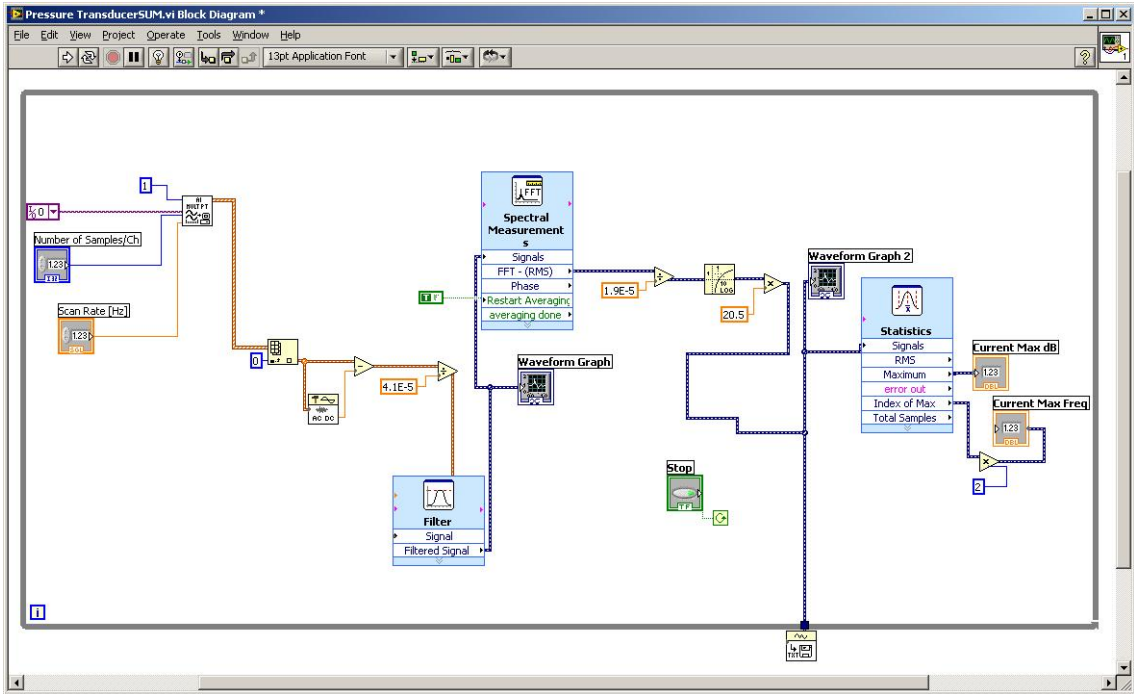


Figure 4.5: Block diagram of configuration for monitoring sound levels

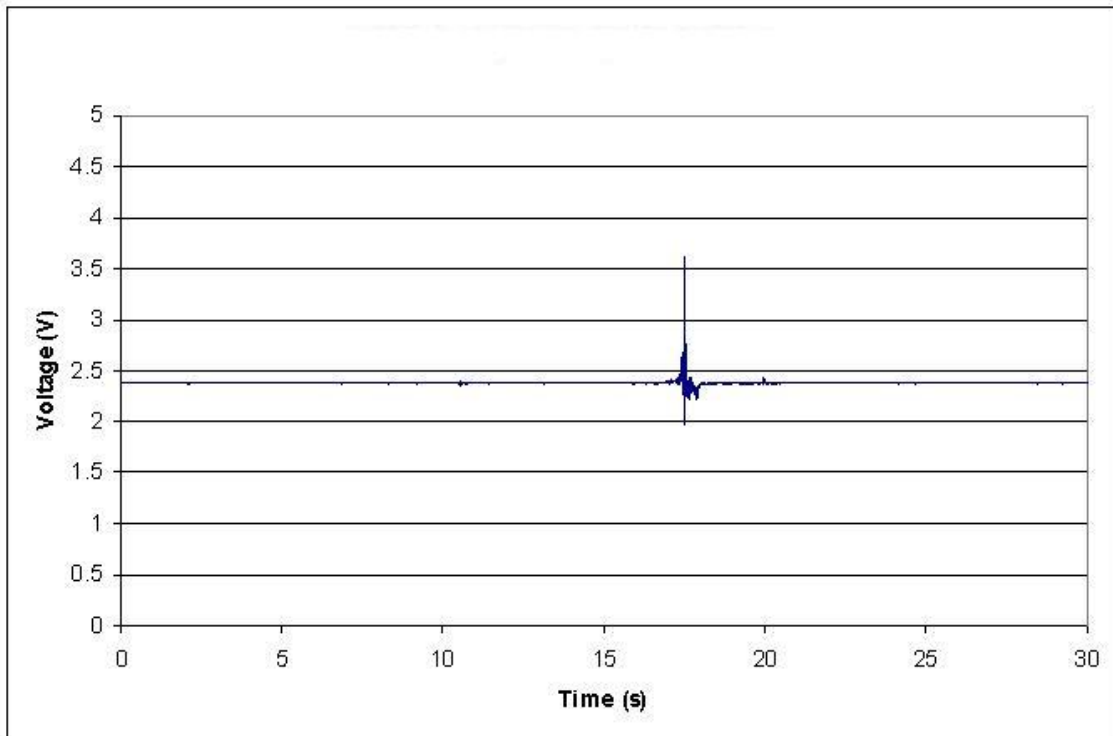


Figure 4.6: Reference gyro frequency sweep from 6kHz to 18kHz

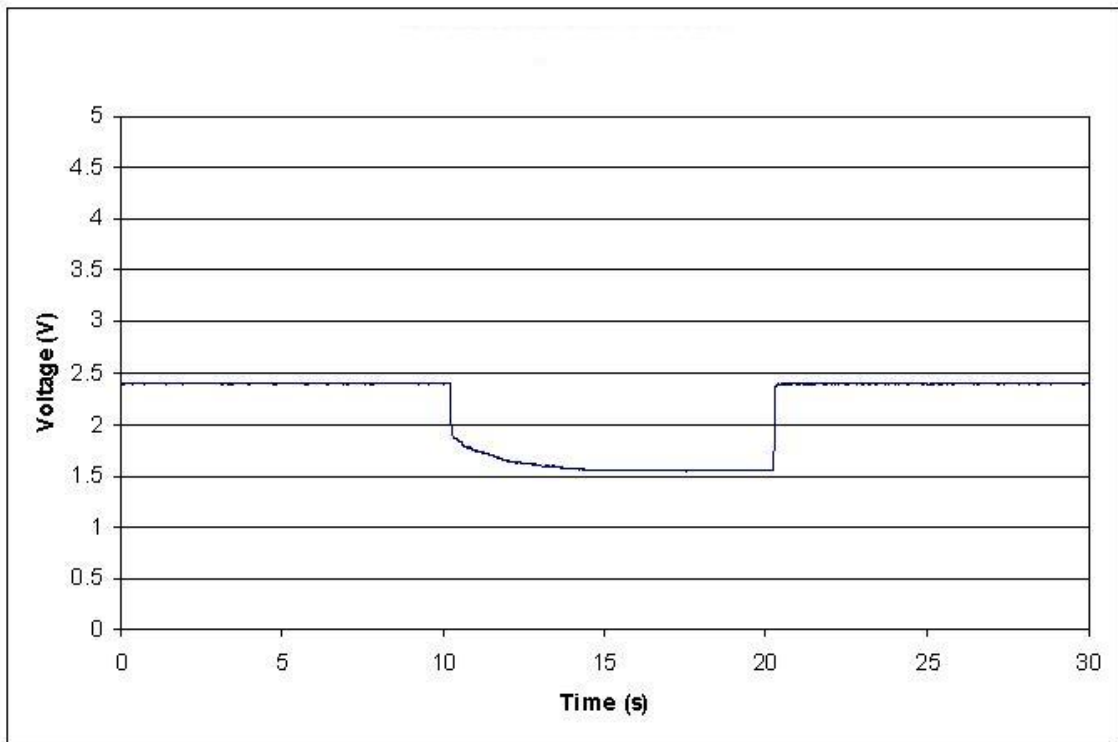


Figure 4.7: Output response from the reference gyroscope at resonant frequency of 13907.77Hz

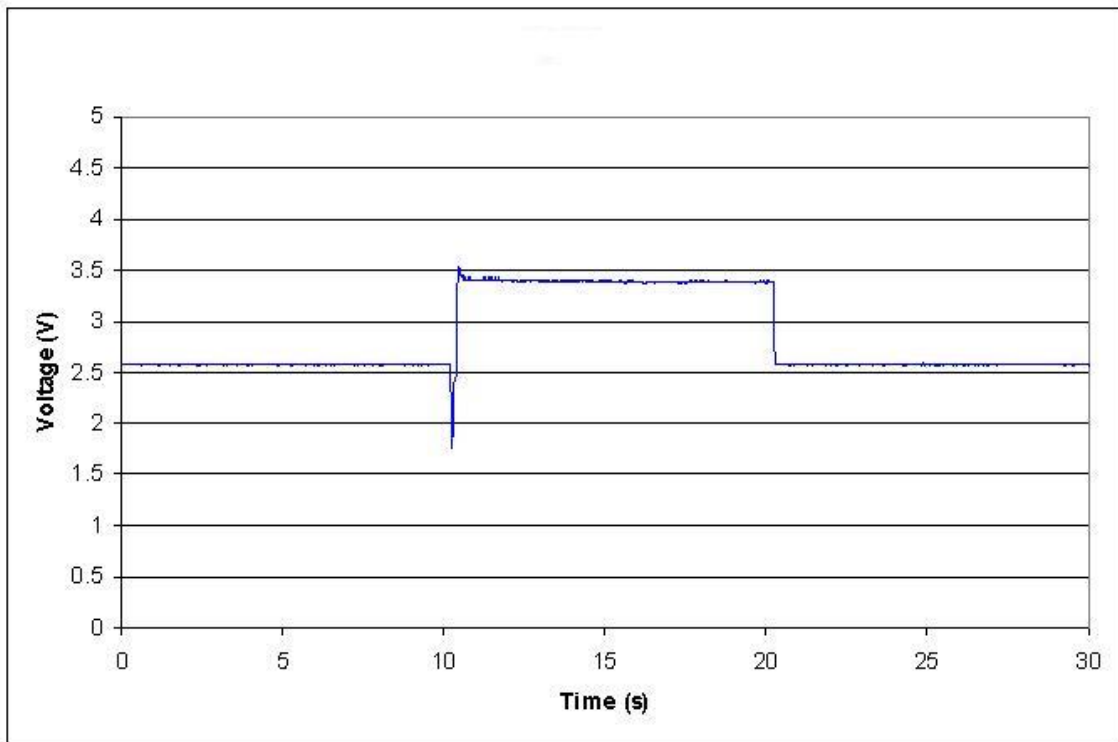


Figure 4.8: Output response from gyro 2 at resonant frequency

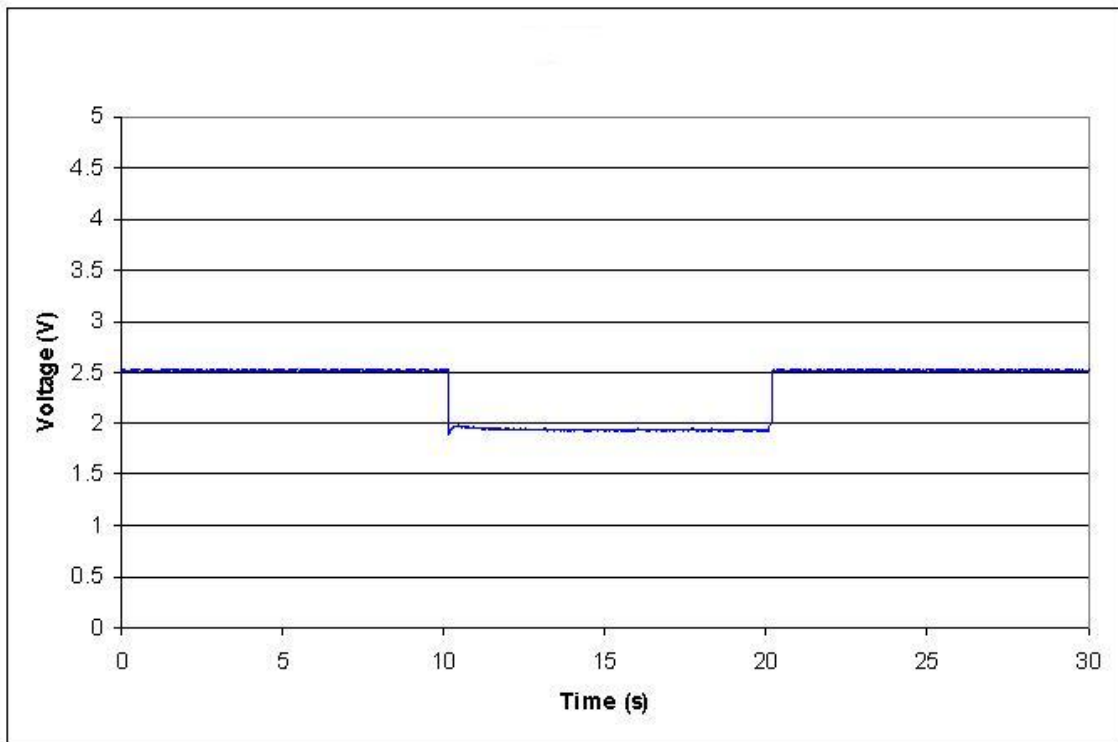


Figure 4.9: Output response from gyro 3 at resonant frequency

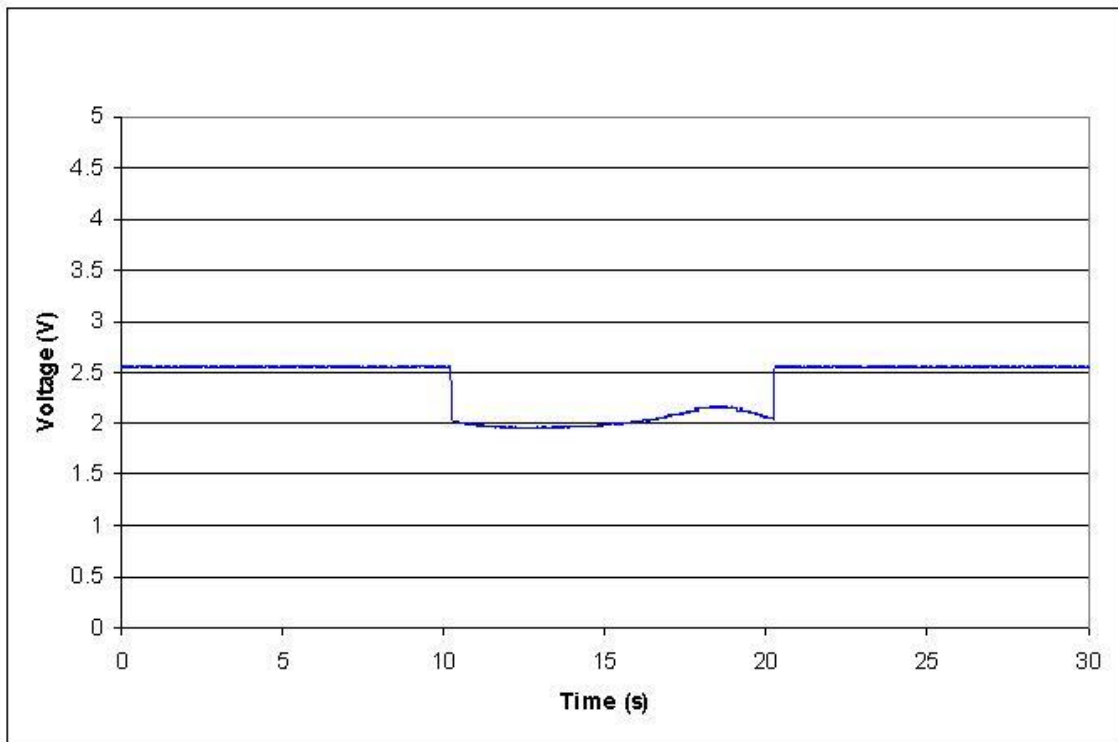


Figure 4.10: Output response from gyro 4 at resonant frequency

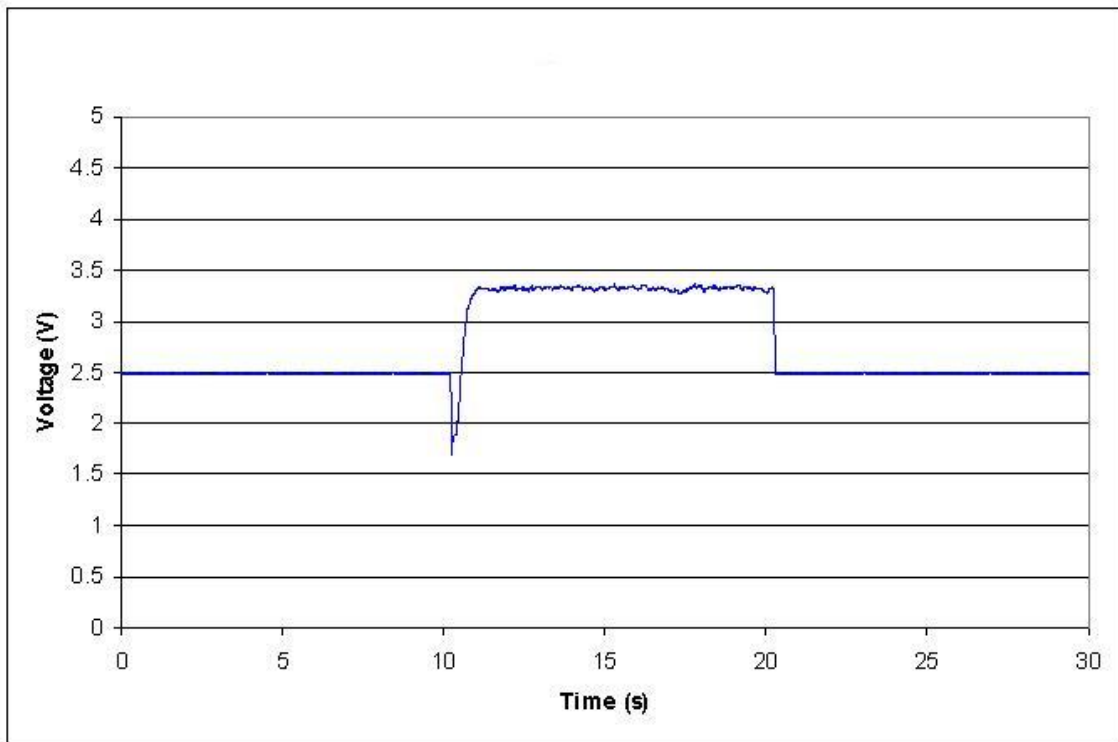


Figure 4.11: Output response from gyro 5 at resonant frequency

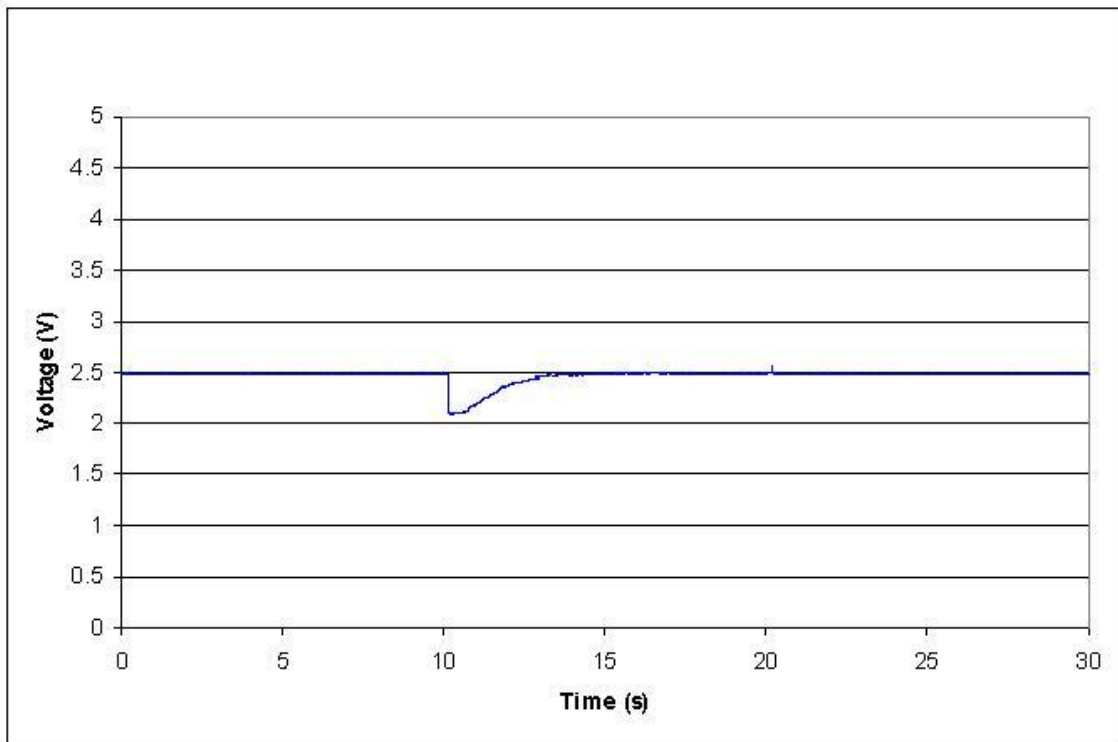


Figure 4.12: Output response from gyro 7 at resonant frequency

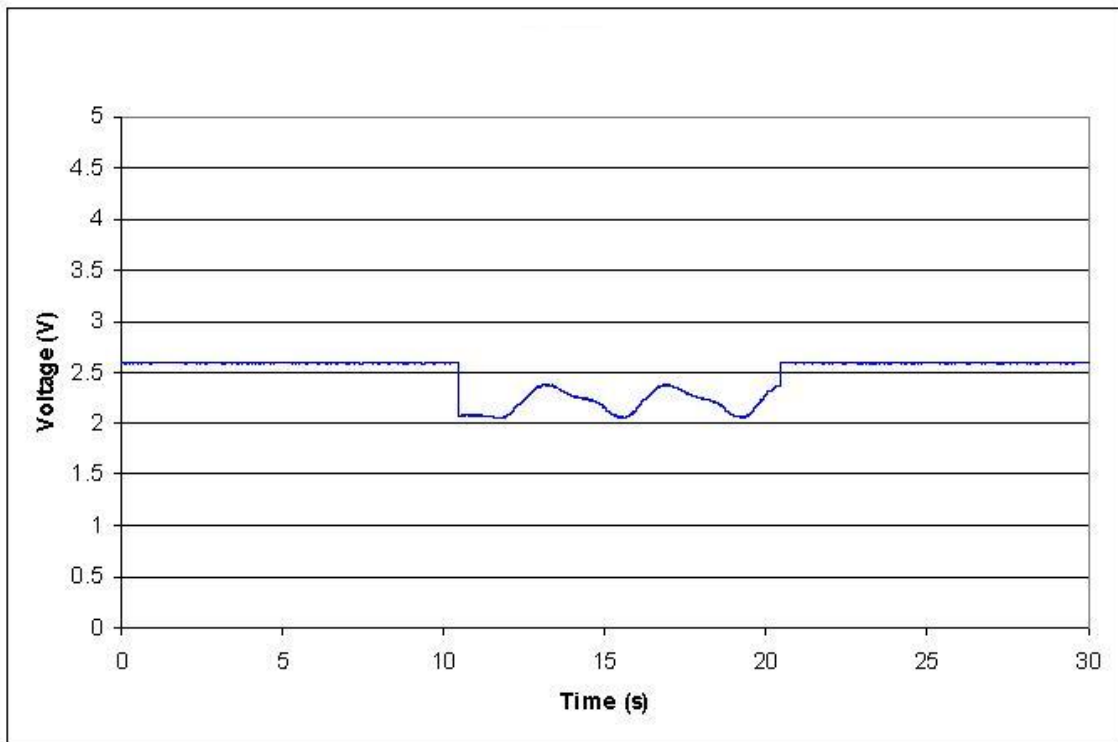


Figure 4.13: Output response from gyro 8 at resonant frequency

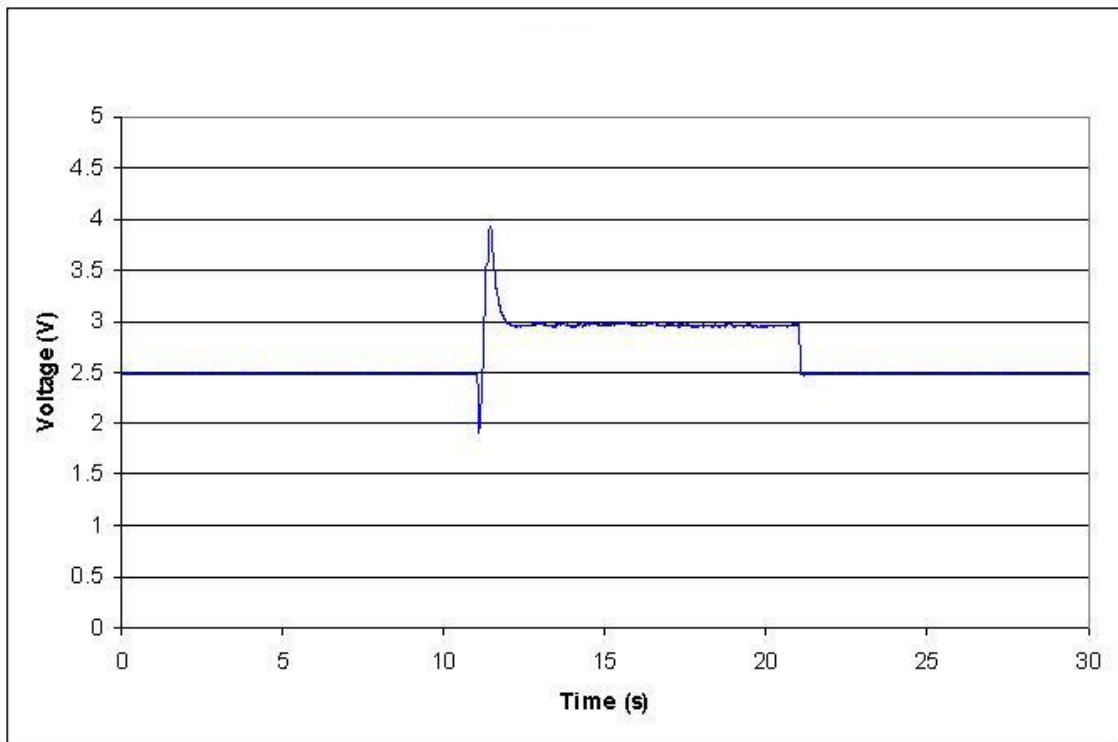


Figure 4.14: Output response from gyro 9 at resonant frequency

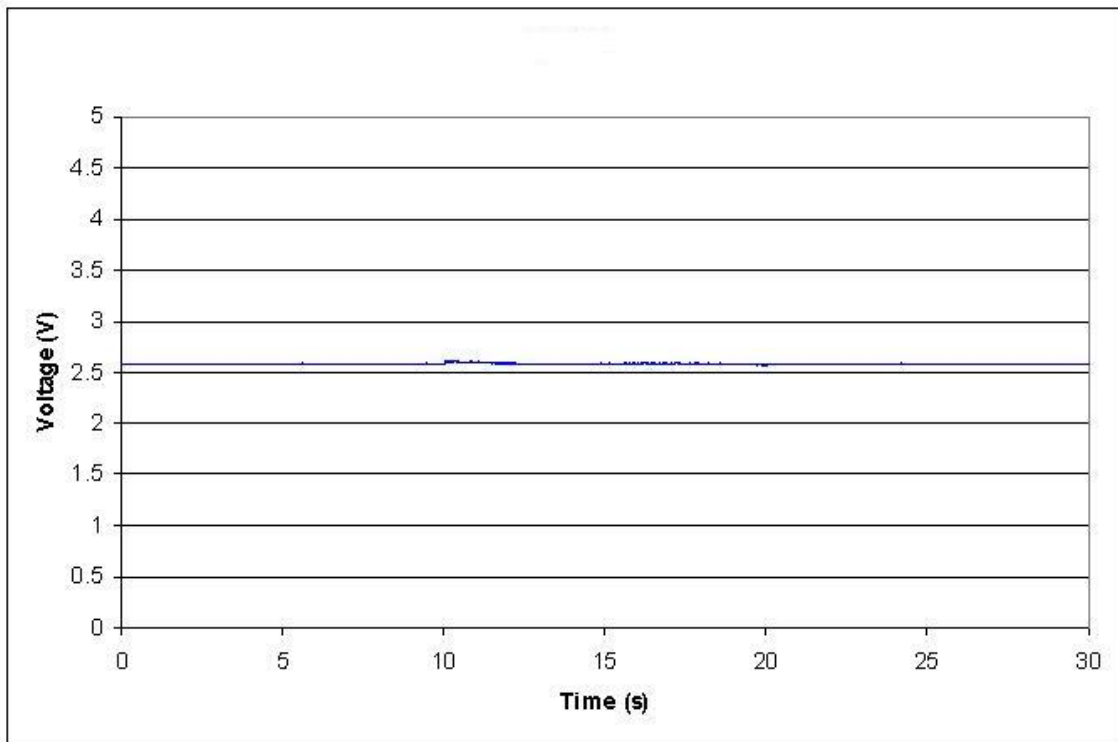


Figure 4.15: Output response from gyro 12 at resonant frequency

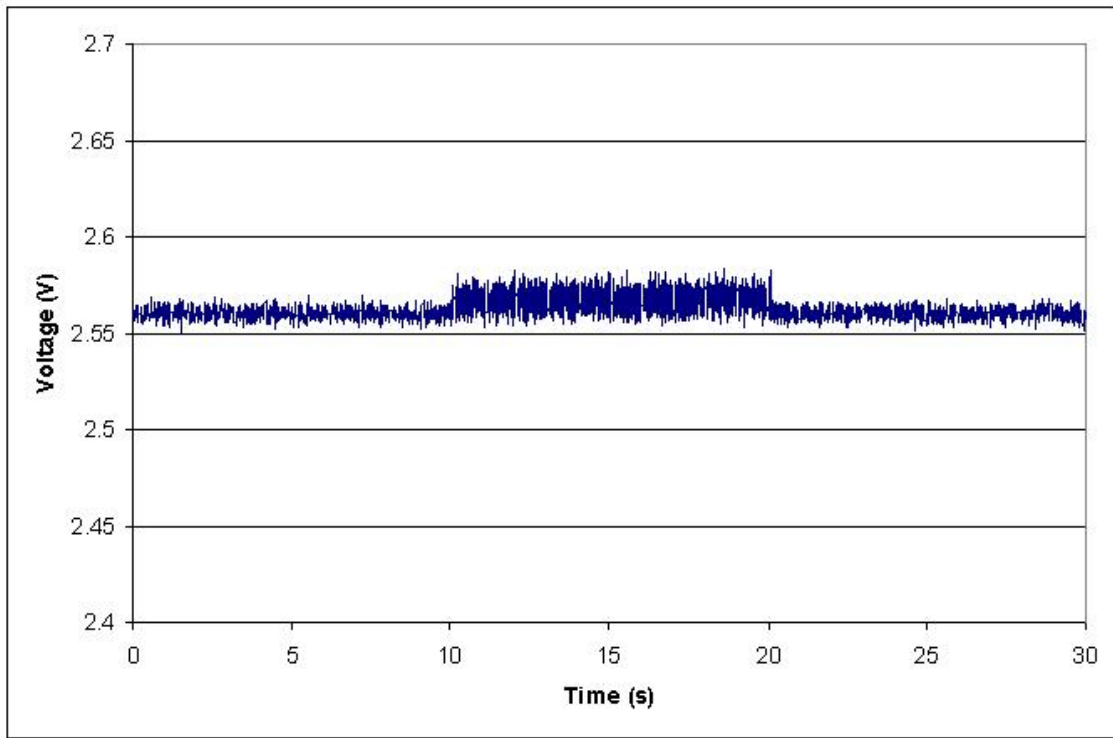


Figure 4.16: Output response from gyro 12 at resonant frequency with y-scale enlarged

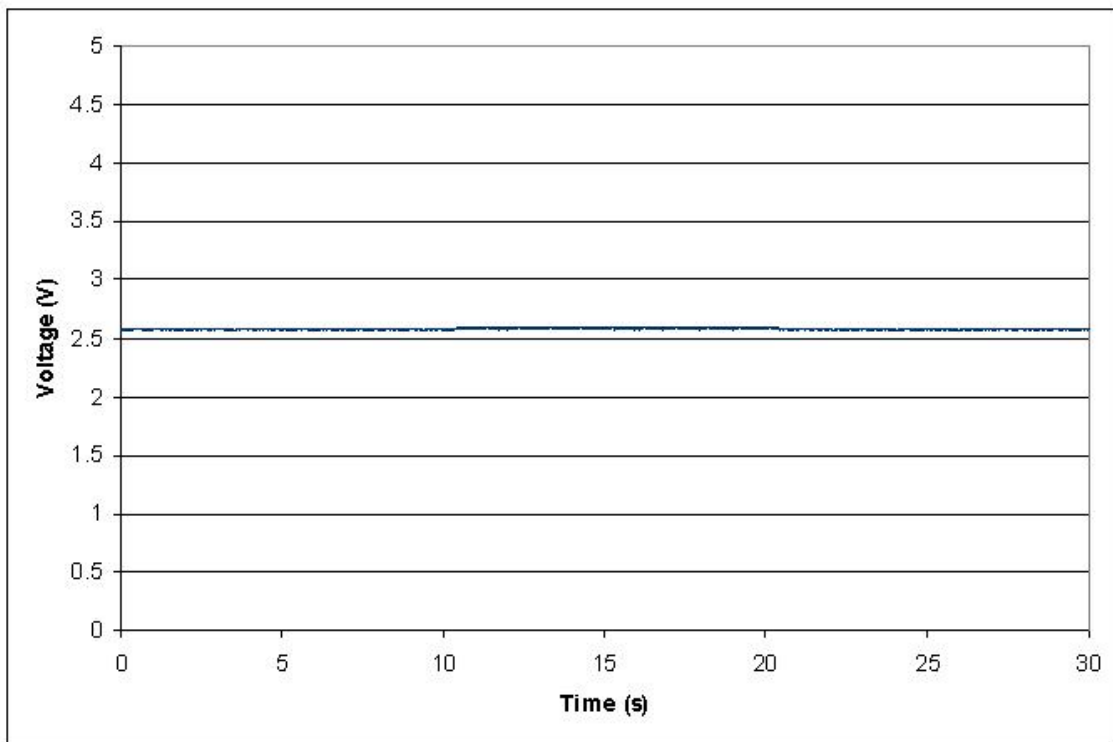


Figure 4.17: Output response from gyro 13 at resonant frequency

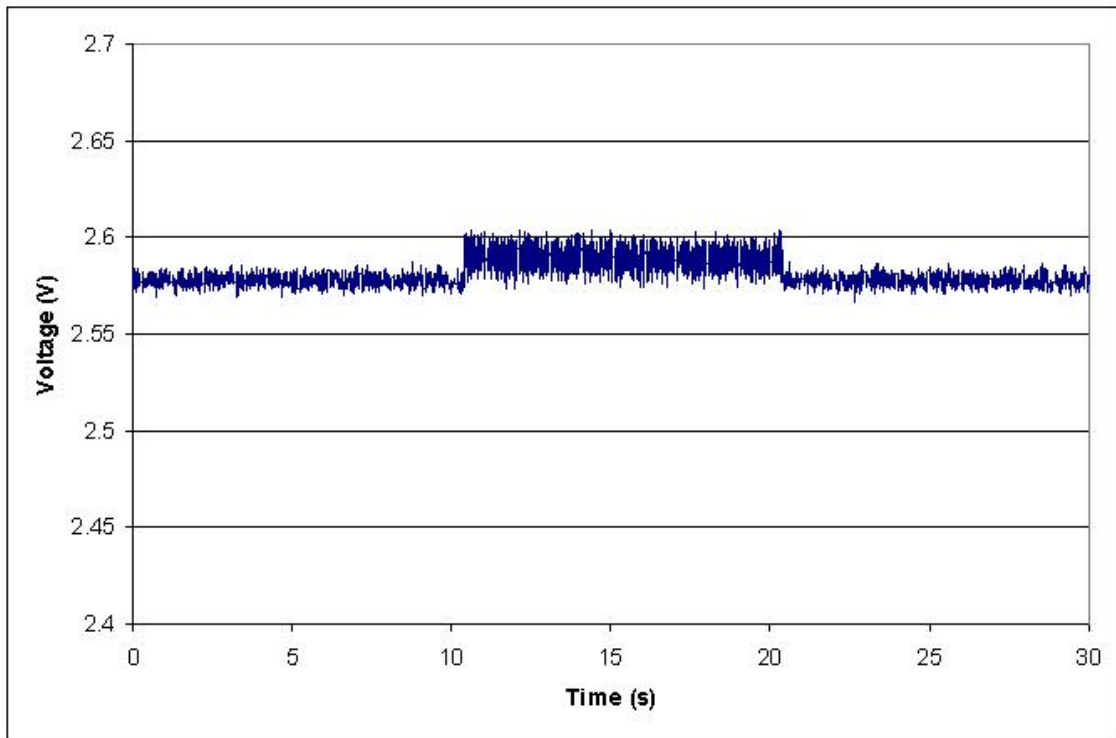


Figure 4.18: Output response from gyro 13 at resonant frequency with y-scale enlarged

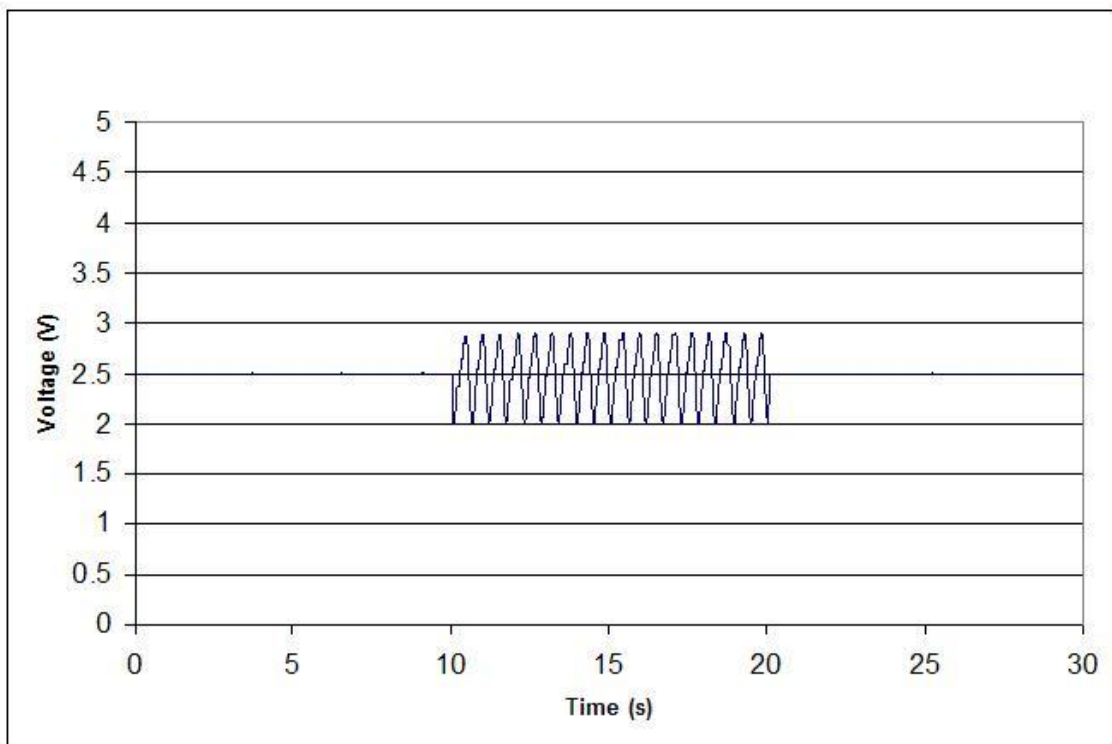


Figure 4.19: Output response from gyro 14 at resonant frequency

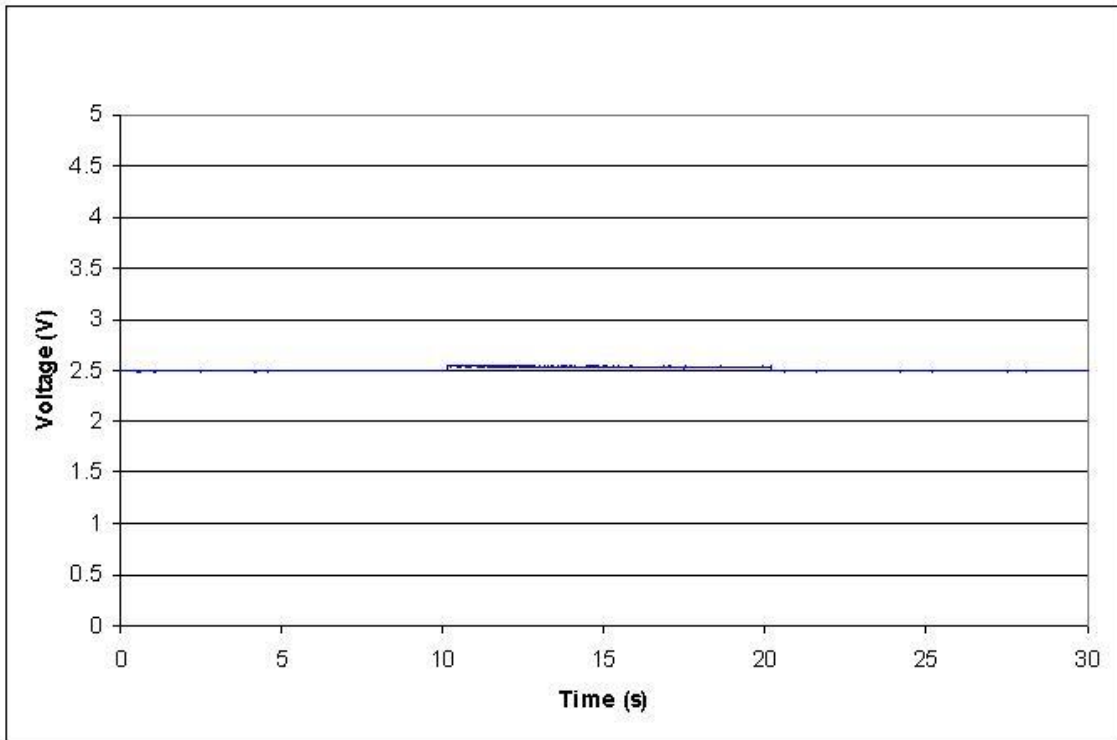


Figure 4.20: Output response from gyro 15 at resonant frequency

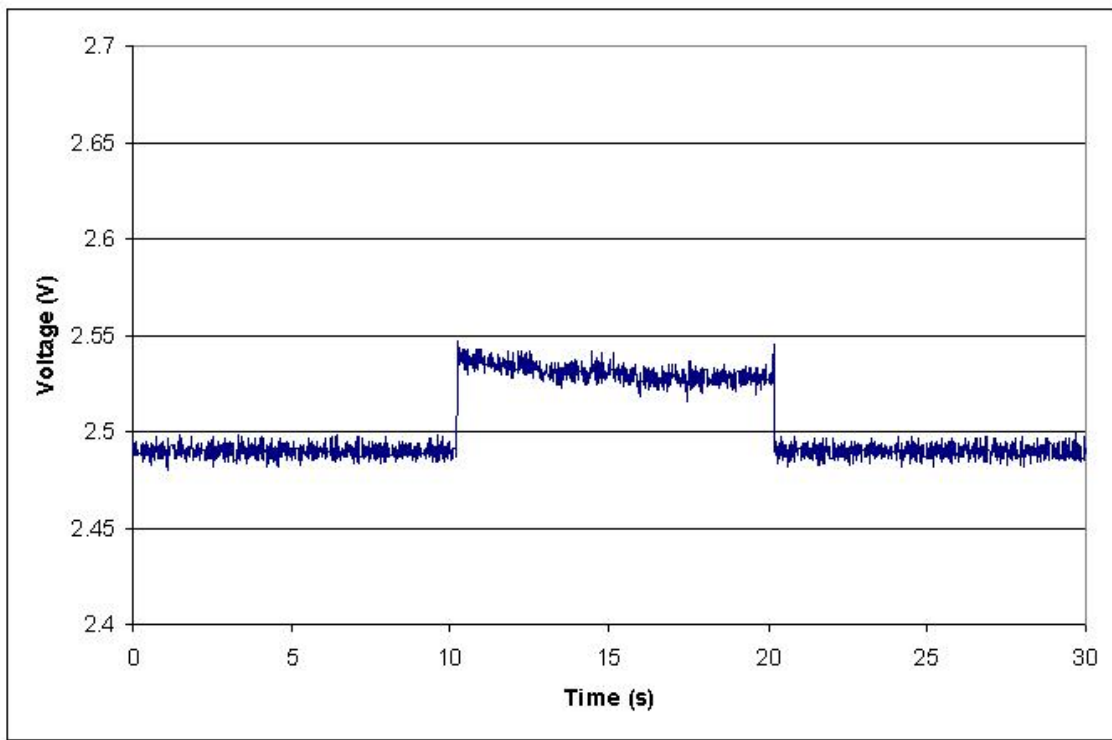


Figure 4.21: Output response from gyro 15 at resonant frequency with y-scale enlarged

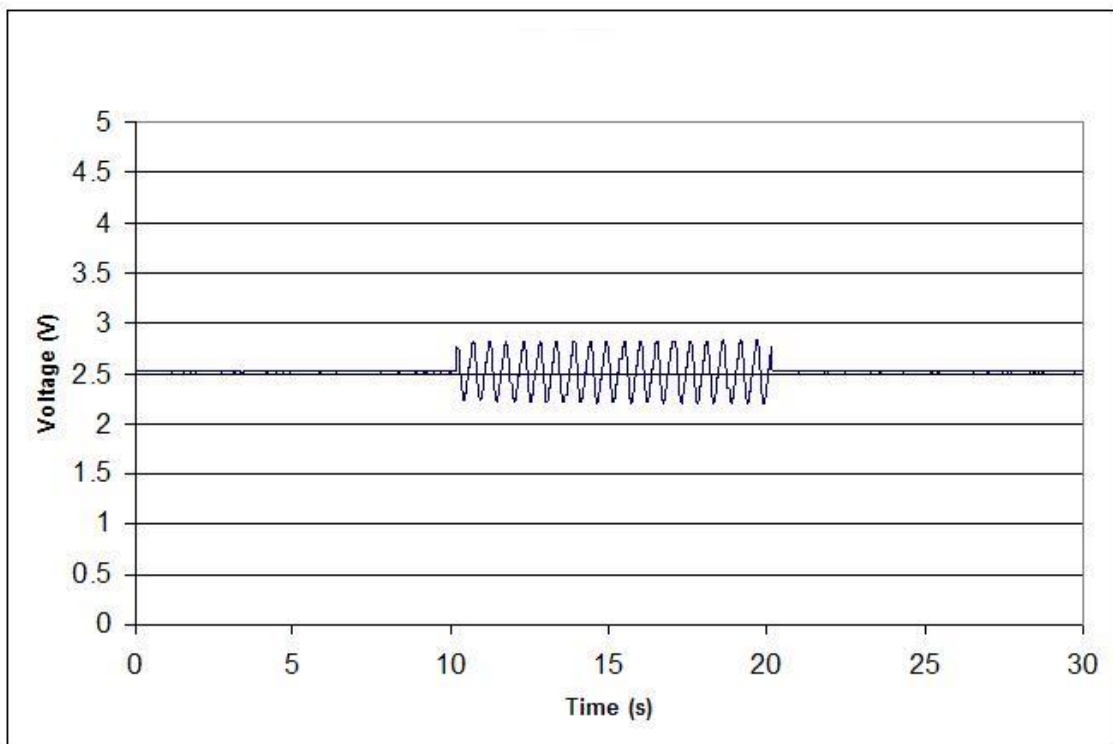


Figure 4.22: Output response from gyro 16 at resonant frequency

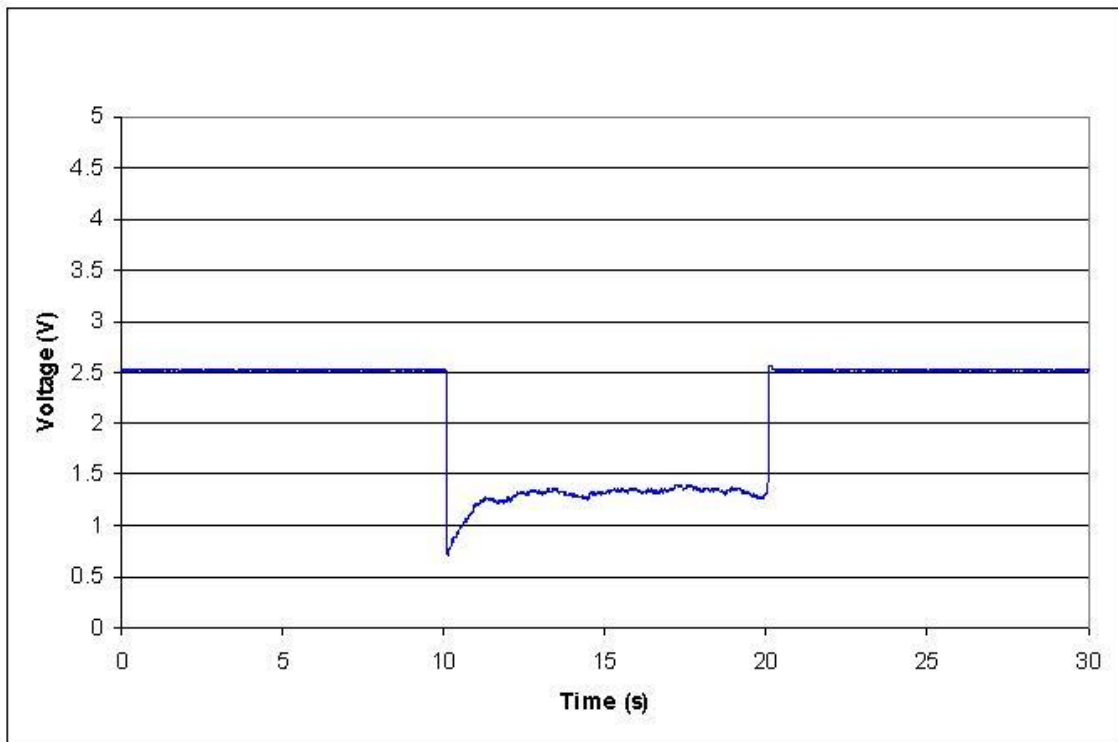


Figure 4.23: Output response from gyro 18 at resonant frequency

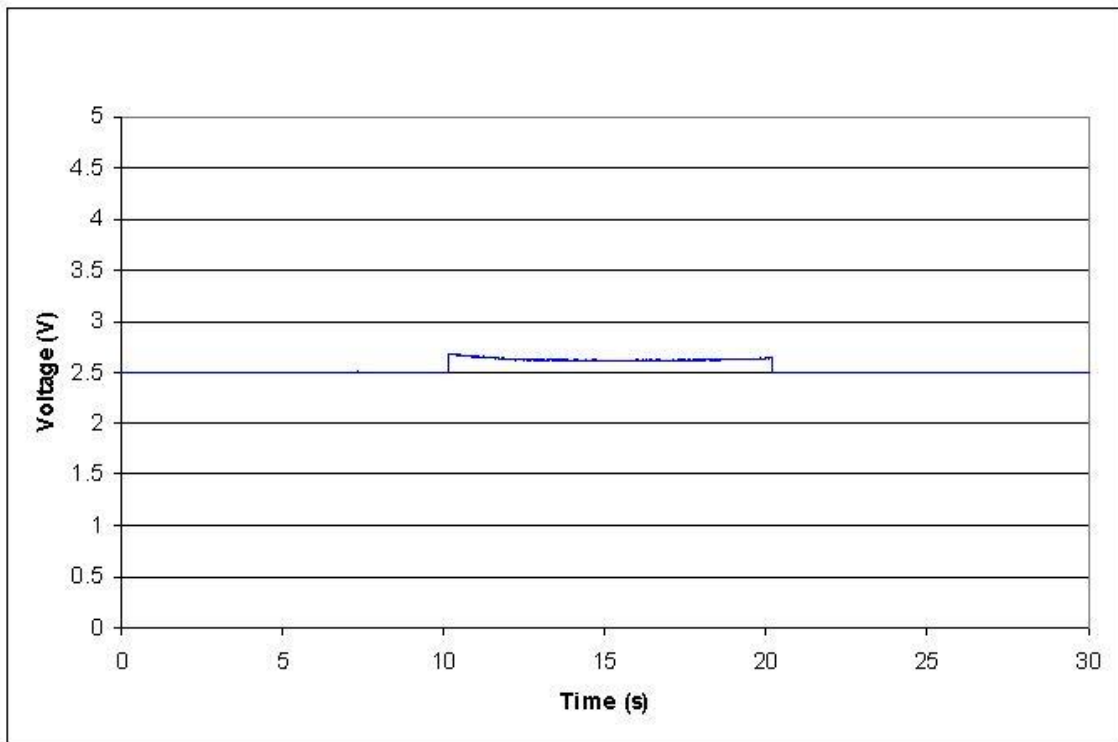


Figure 4.24: Output response from gyro 19 at resonant frequency

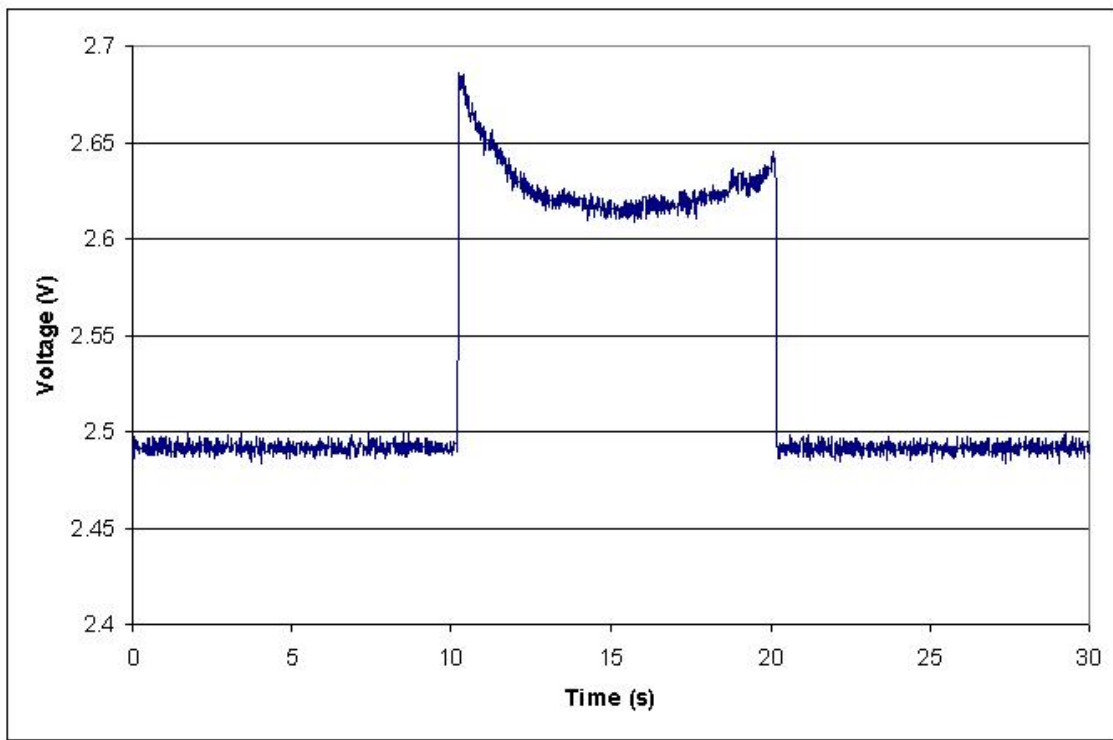


Figure 4.25: Output response from gyro 19 at resonant frequency with y-scale enlarged

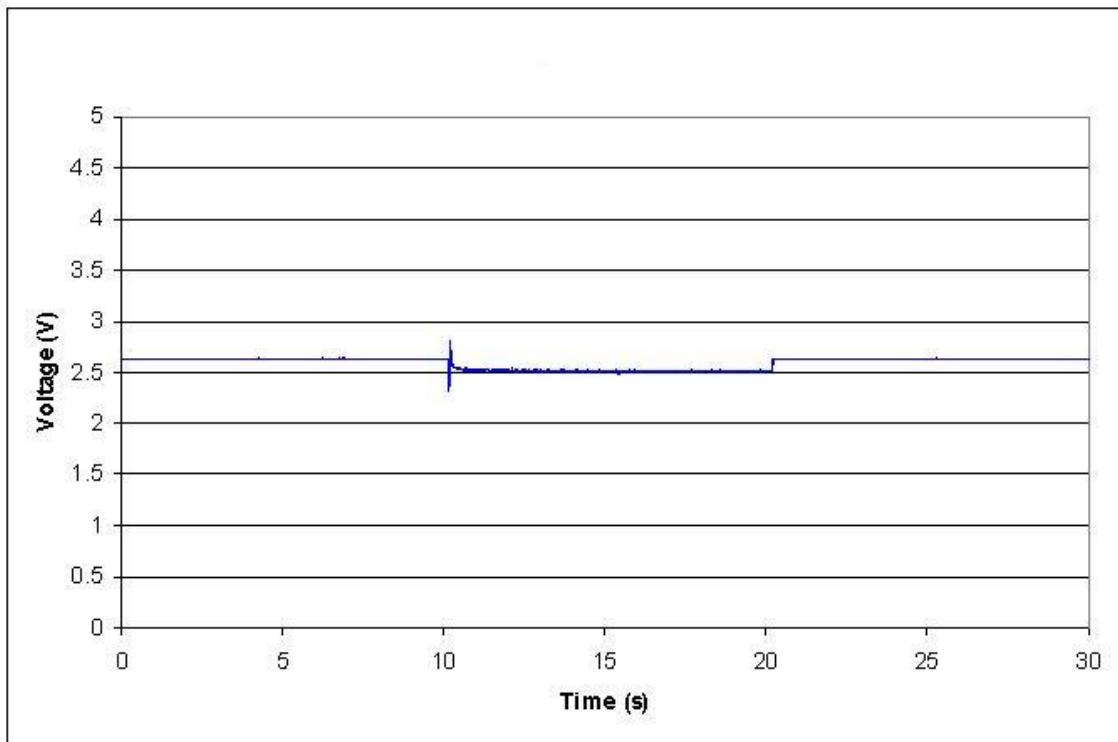


Figure 4.26: Output response from gyro 20 at resonant frequency

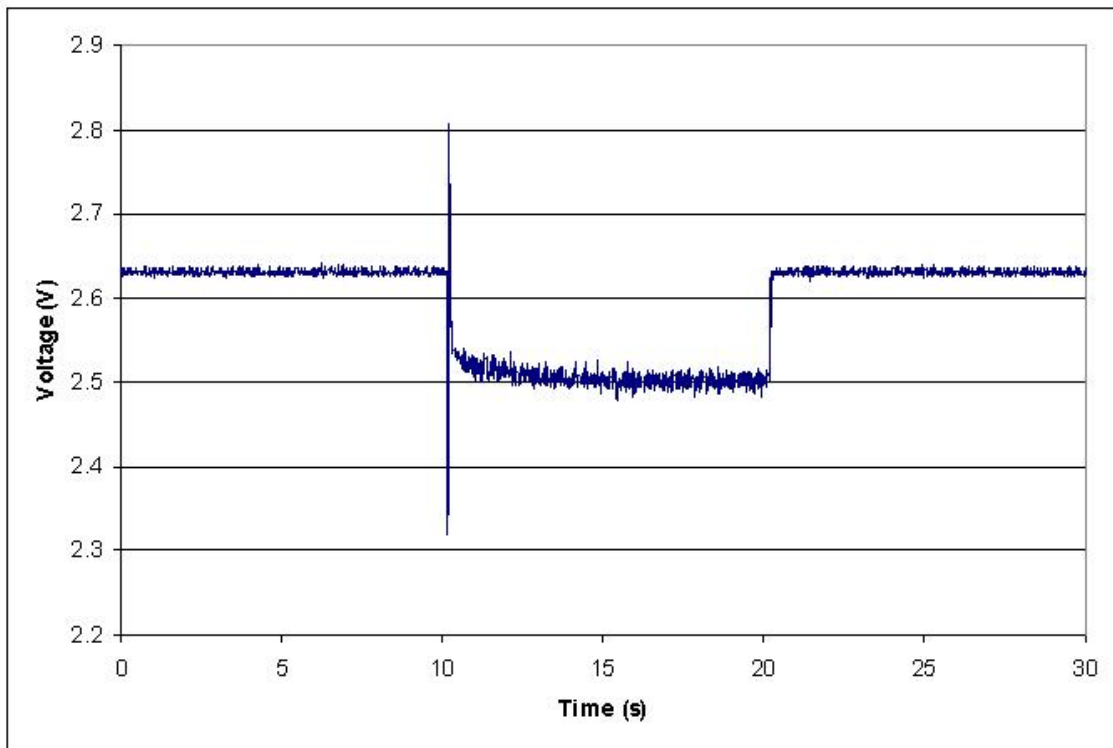


Figure 4.27: Output response from gyro 20 at resonant frequency with y-scale enlarged

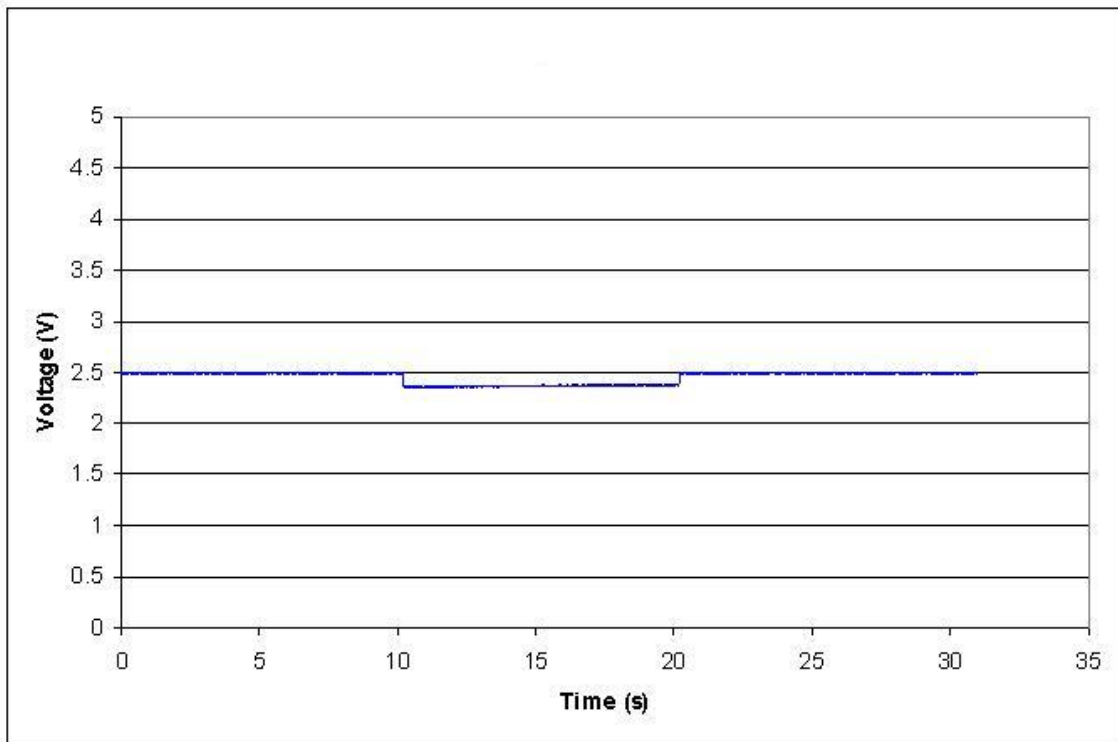


Figure 4.28: Output response from gyro 21 at resonant frequency

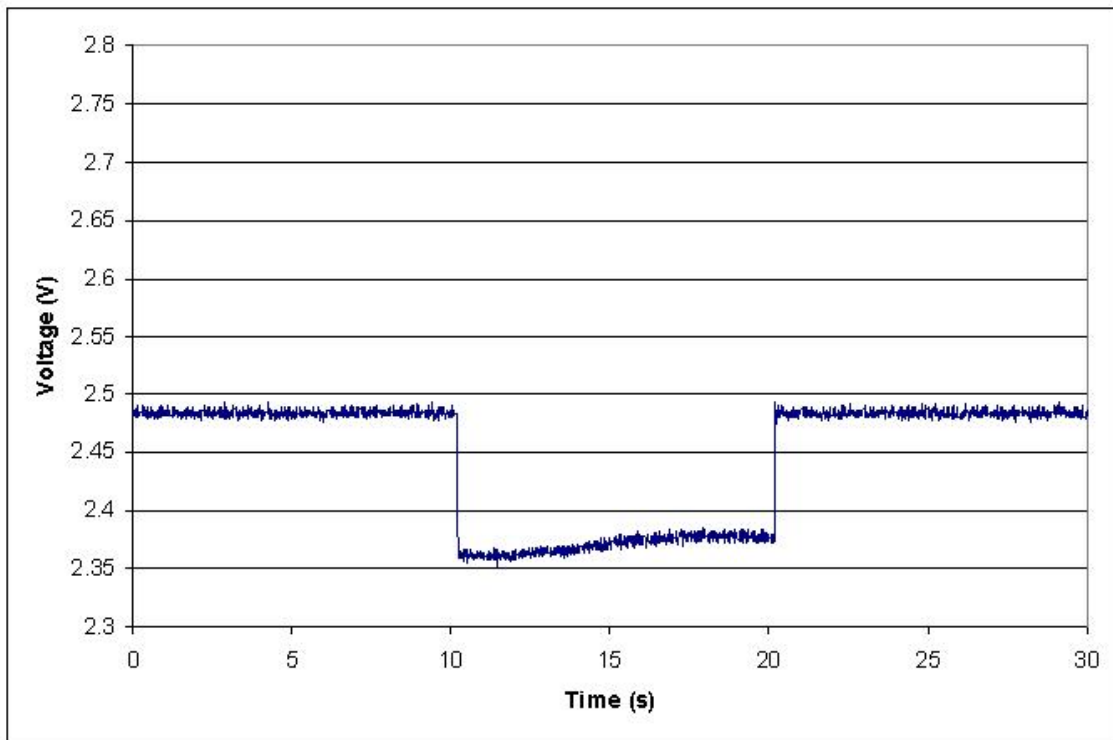


Figure 4.29: Output response from gyro 21 at resonant frequency with y-scale enlarged

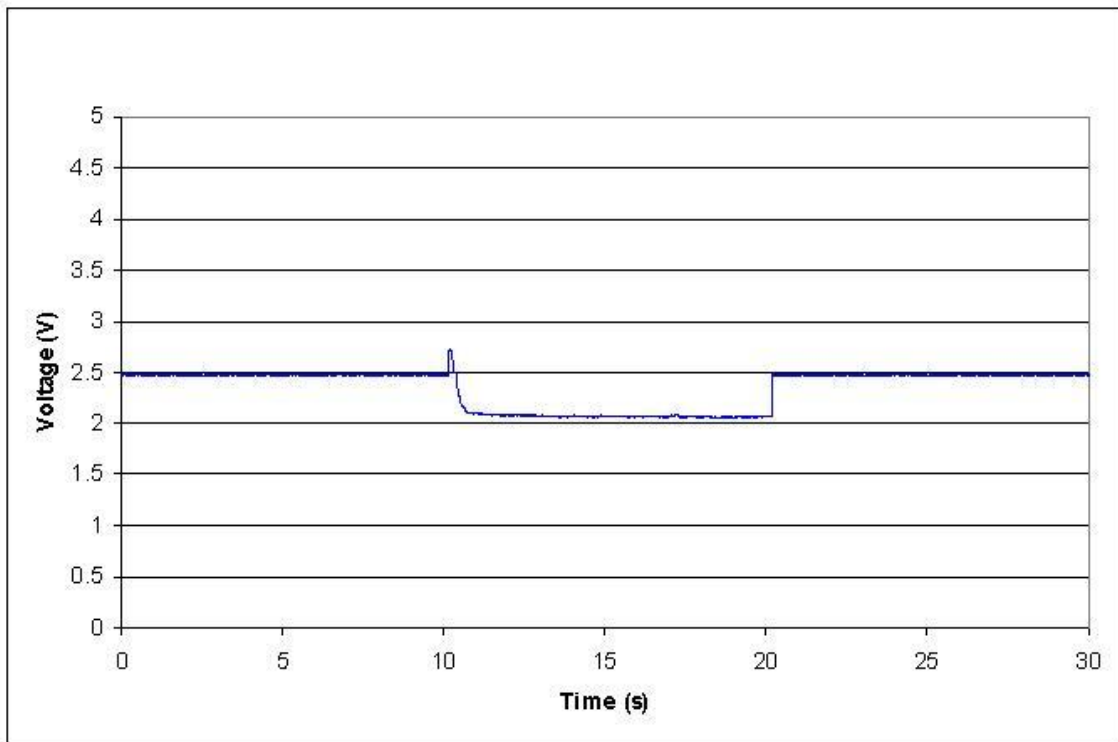


Figure 4.30: Output response from gyro 22 at resonant frequency

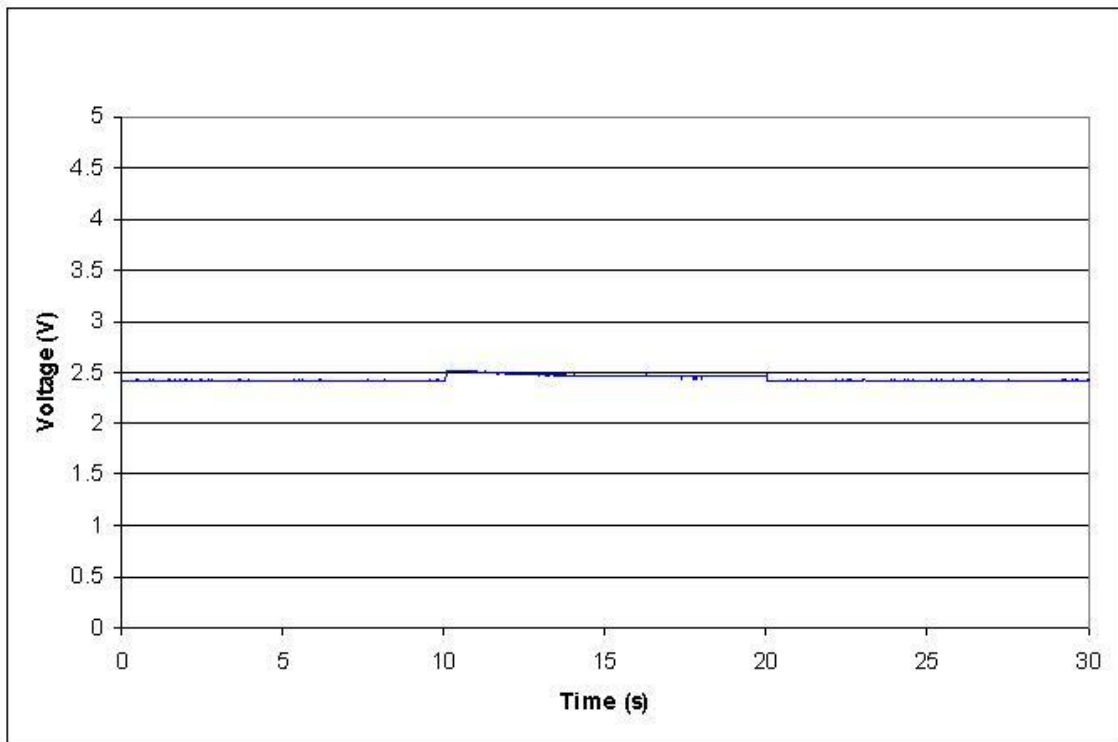


Figure 4.31: Output response from gyro 23 at resonant frequency

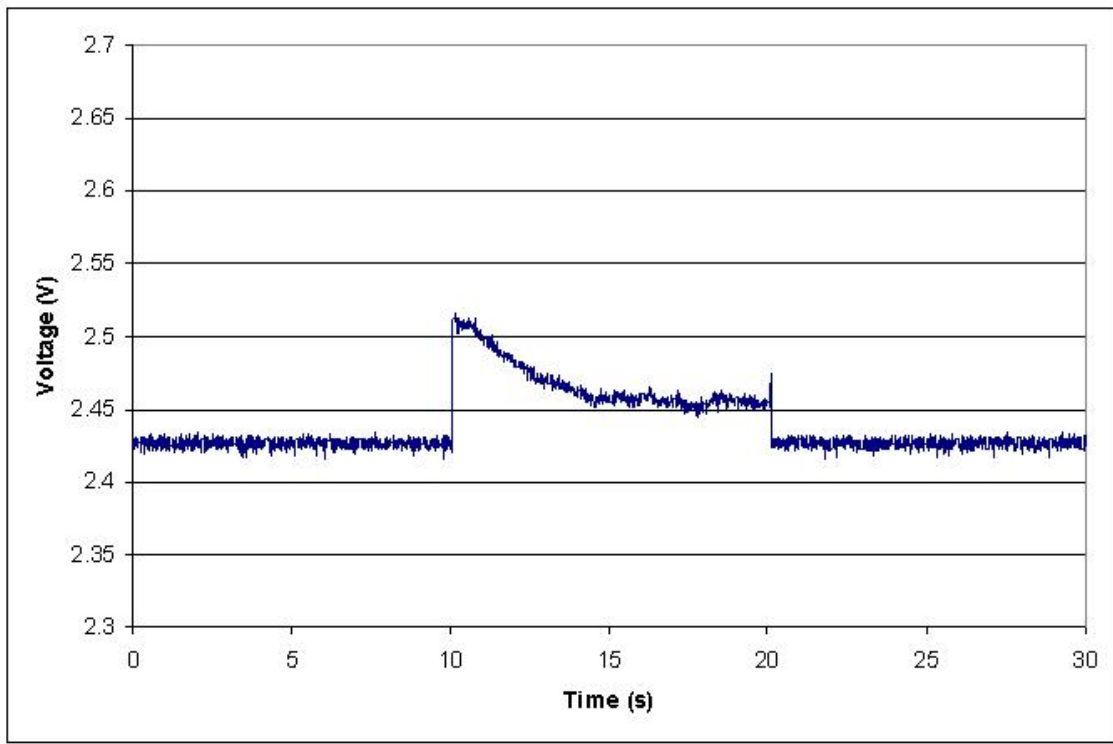


Figure 4.32: Output response from gyro 23 at resonant frequency with y-scale enlarged

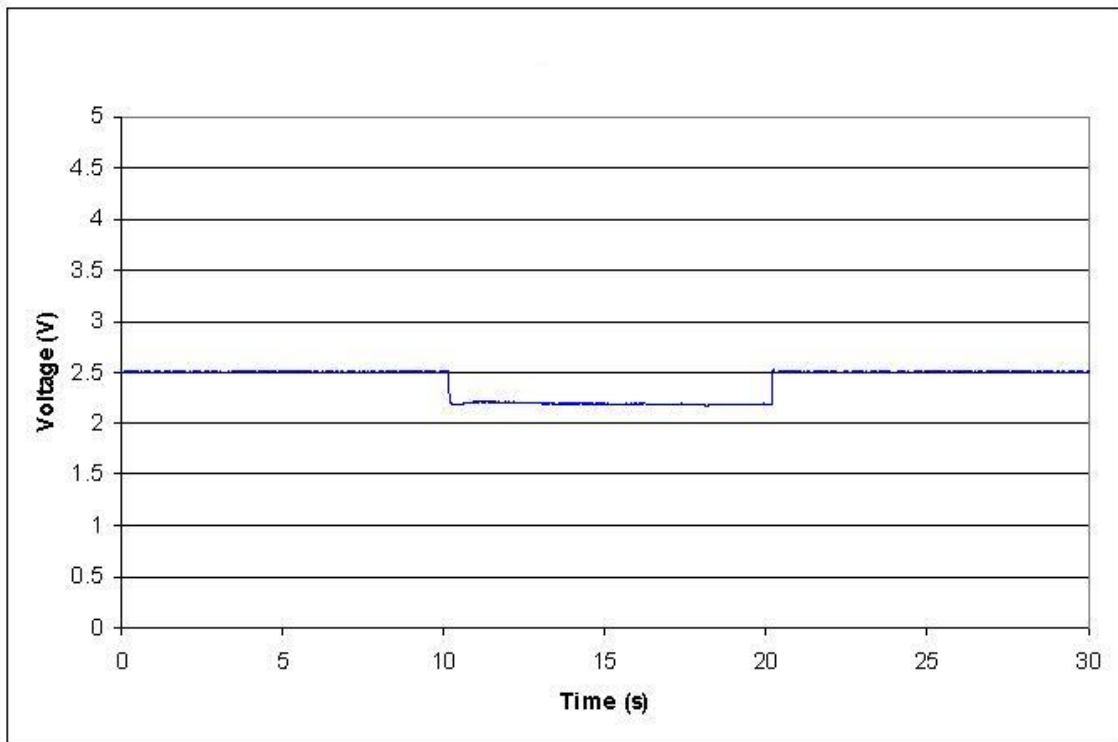


Figure 4.33: Output response from gyro 24 at resonant frequency



Figure 4.34: Photograph of foam samples used during the experimental testing

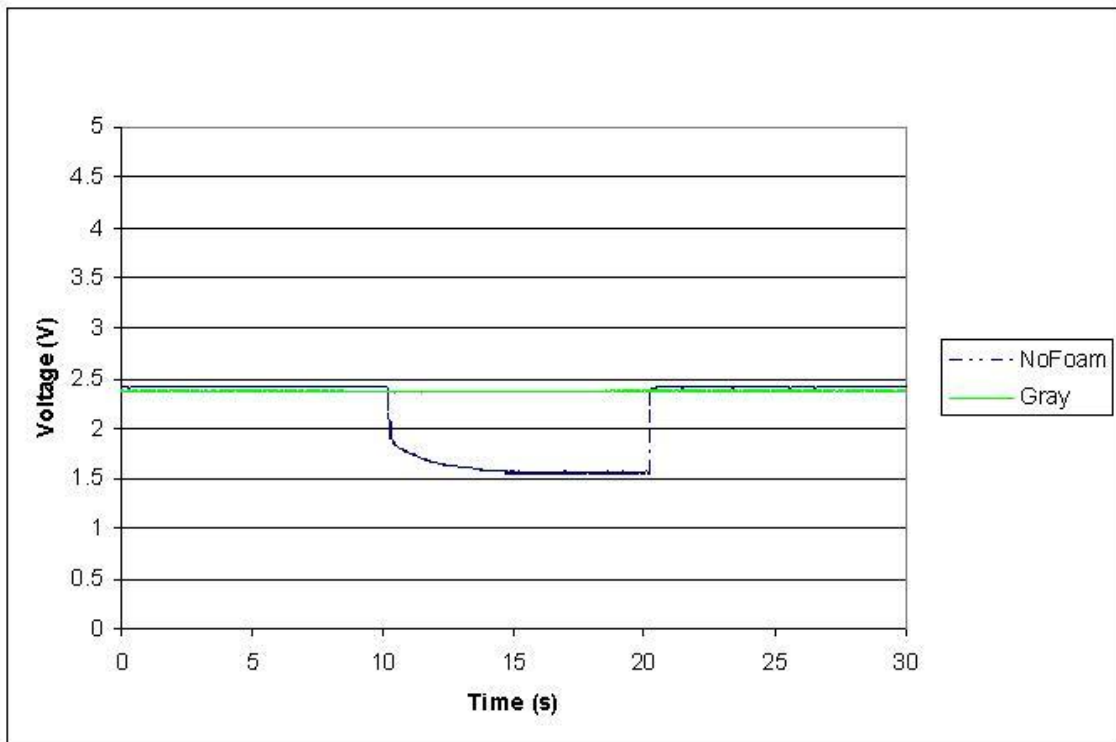


Figure 4.35: Output responses from the reference gyro without foam and with gray foam

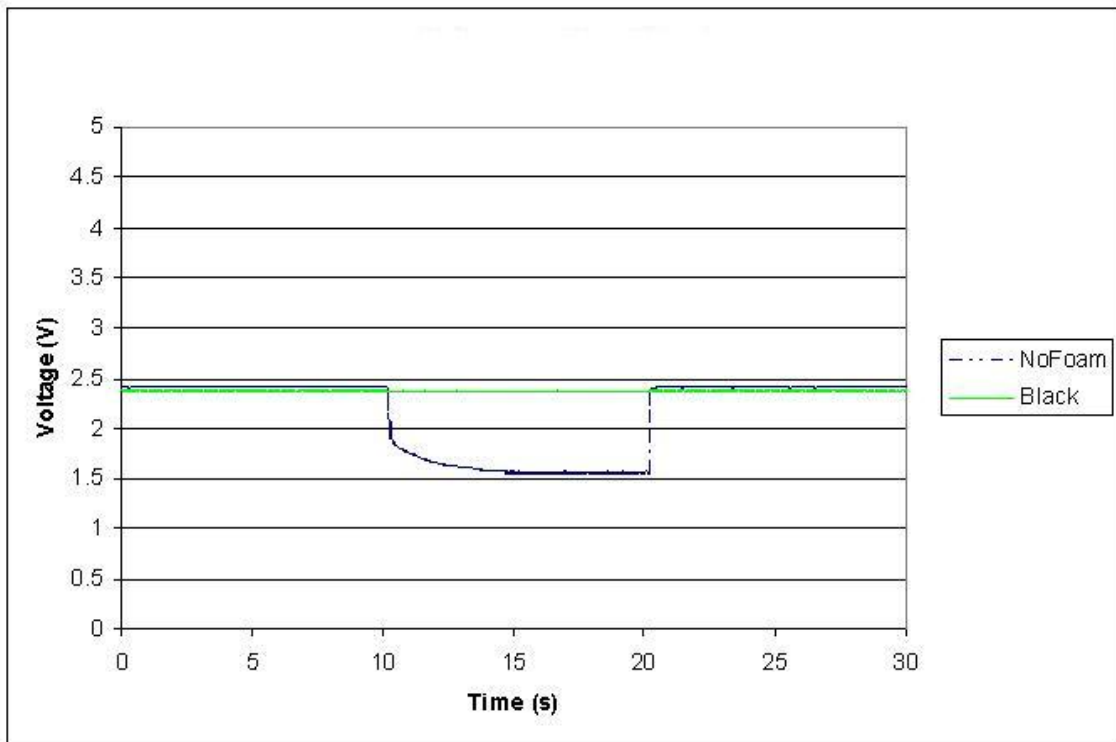


Figure 4.36: Output responses from the reference gyro without foam and with black foam

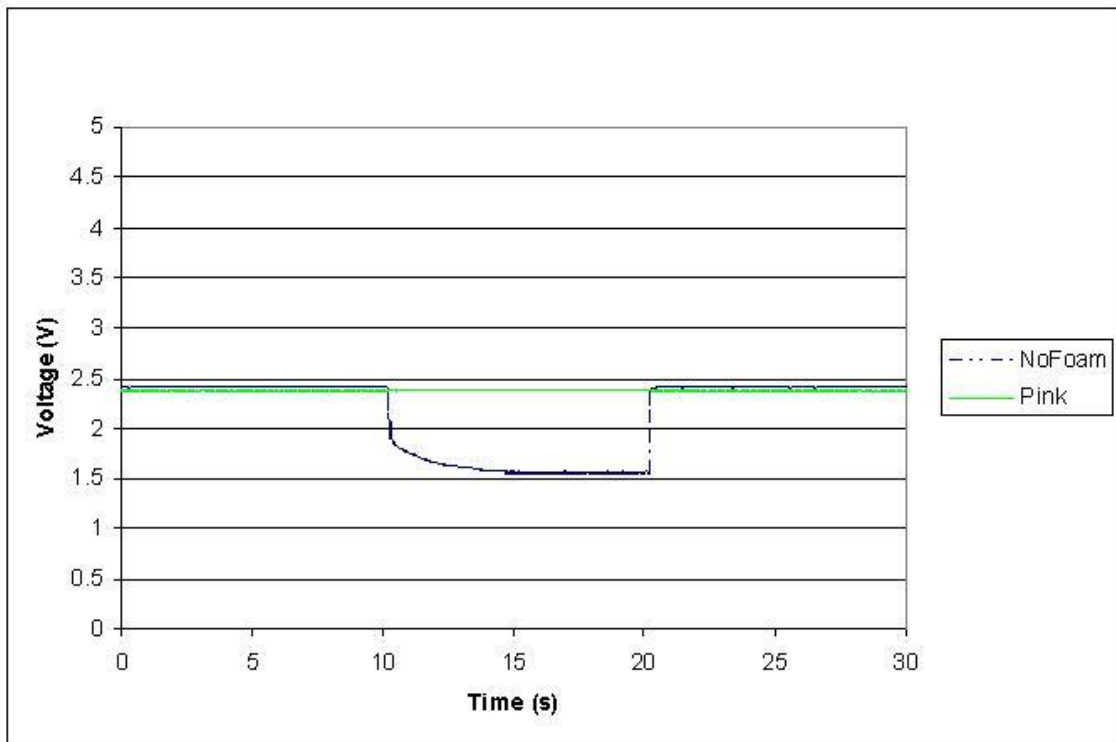


Figure 4.37: Output responses from the reference gyro without foam and with pink foam

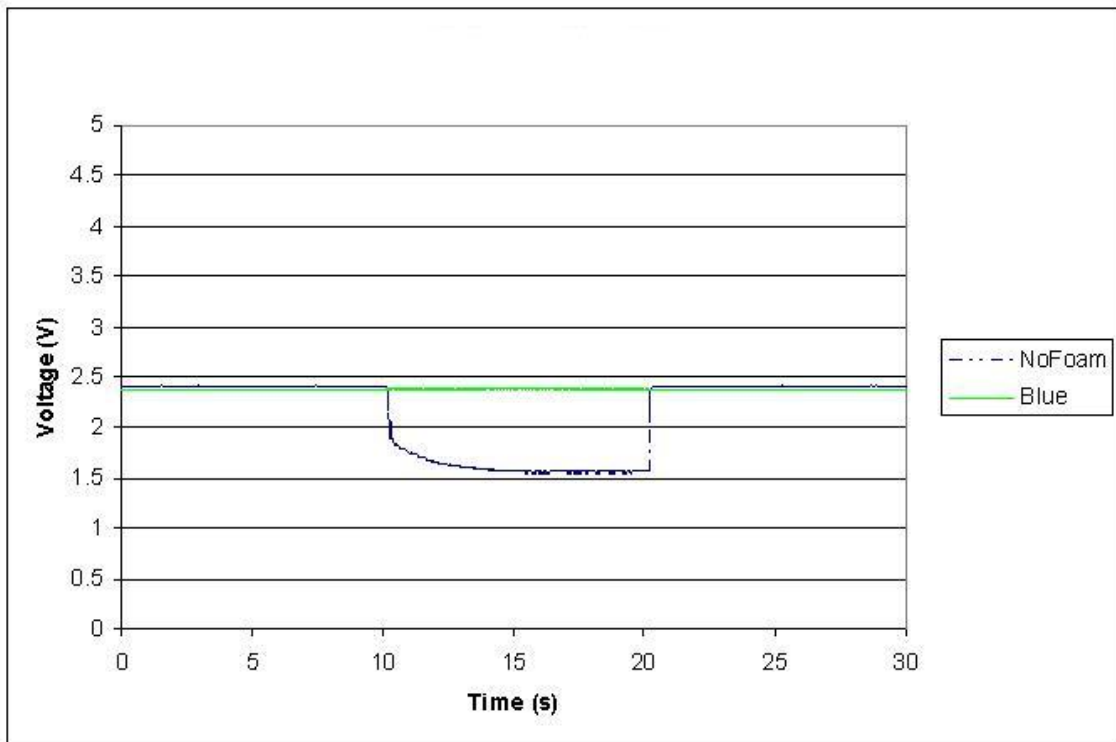


Figure 4.38: Output responses from the reference gyro without foam and with blue foam

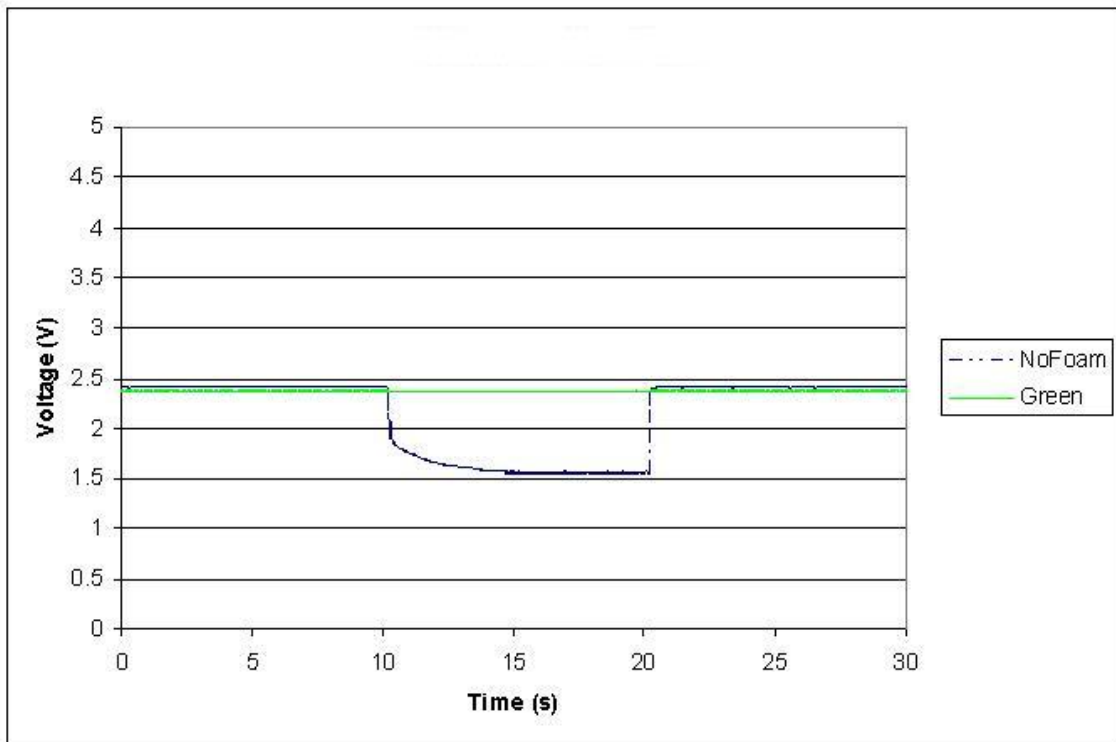


Figure 4.39: Output responses from the reference gyro without foam and with green foam

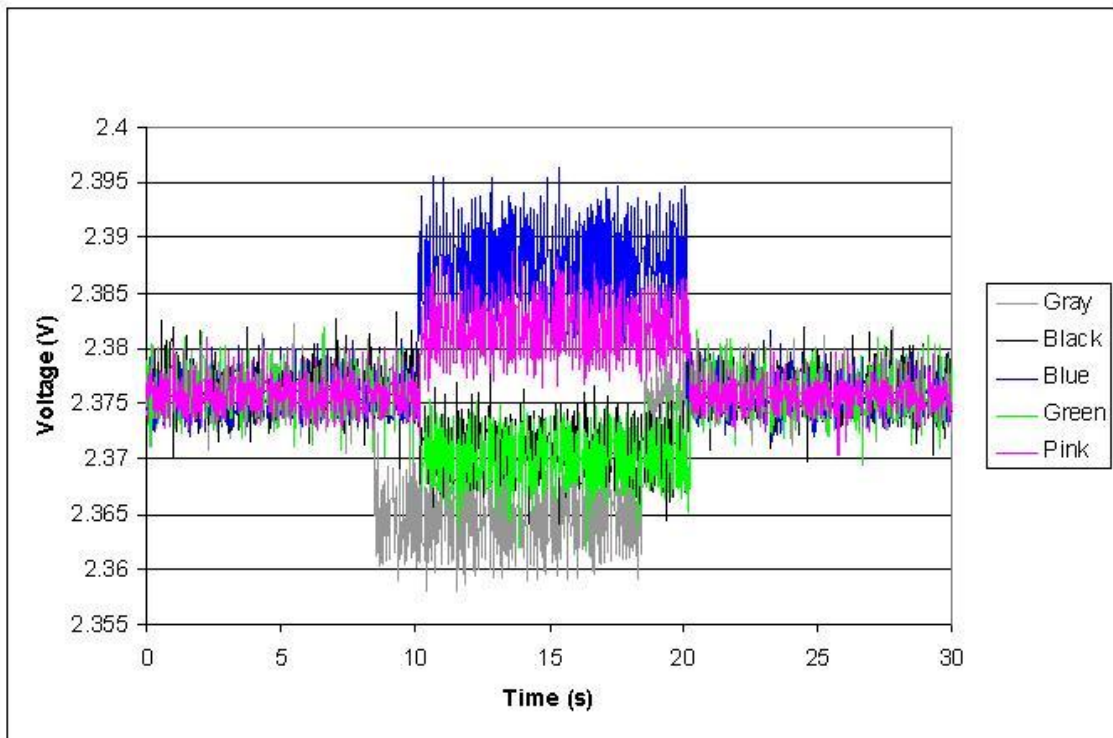


Figure 4.40: A comparison of the reference gyro's output signal for all foams

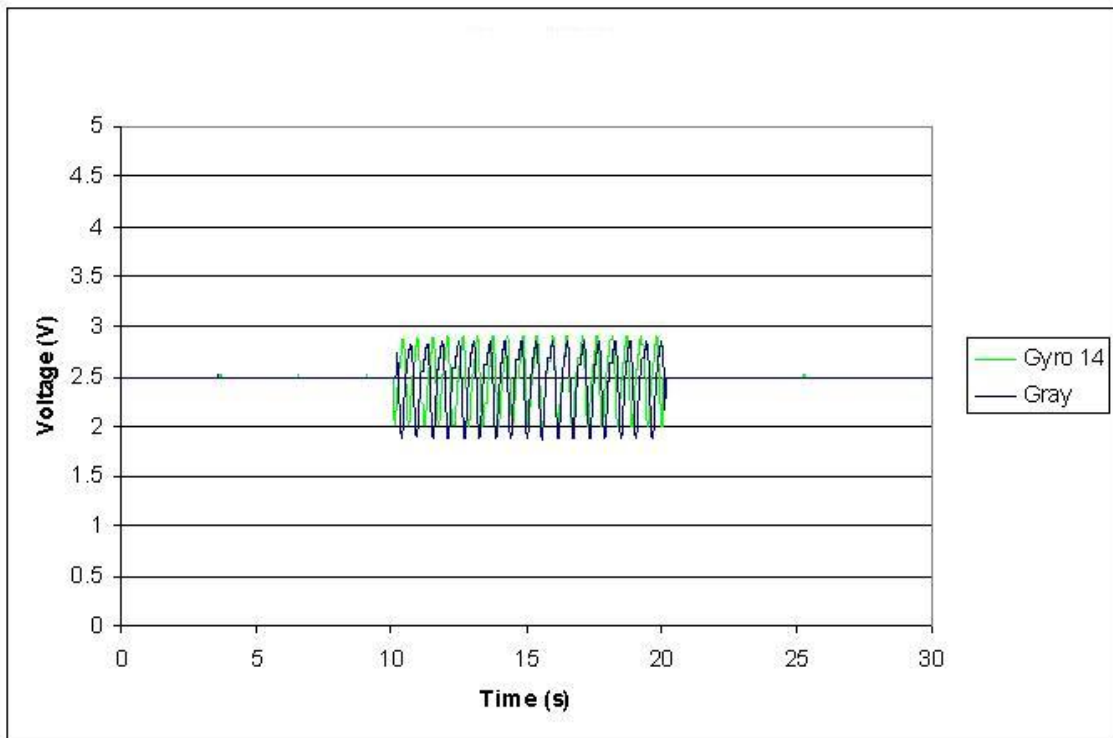


Figure 4.41: Output responses from gyro 14 without foam and with gray foam

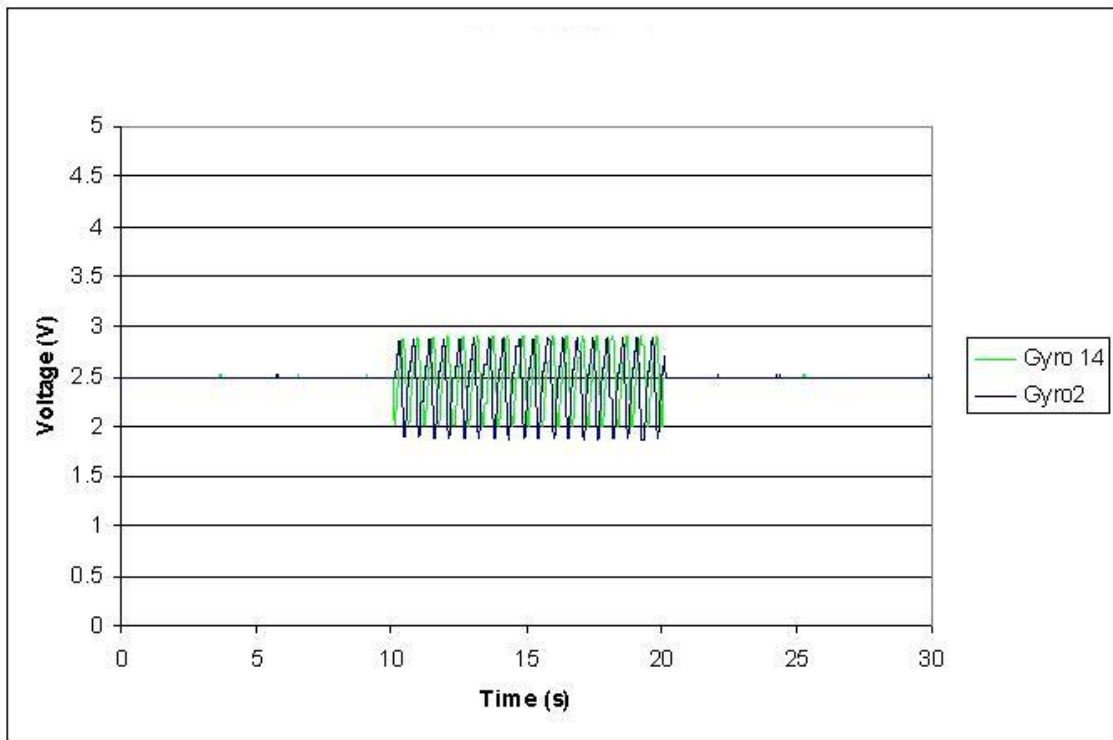


Figure 4.42: Output responses from gyro 14 without foam and with black foam

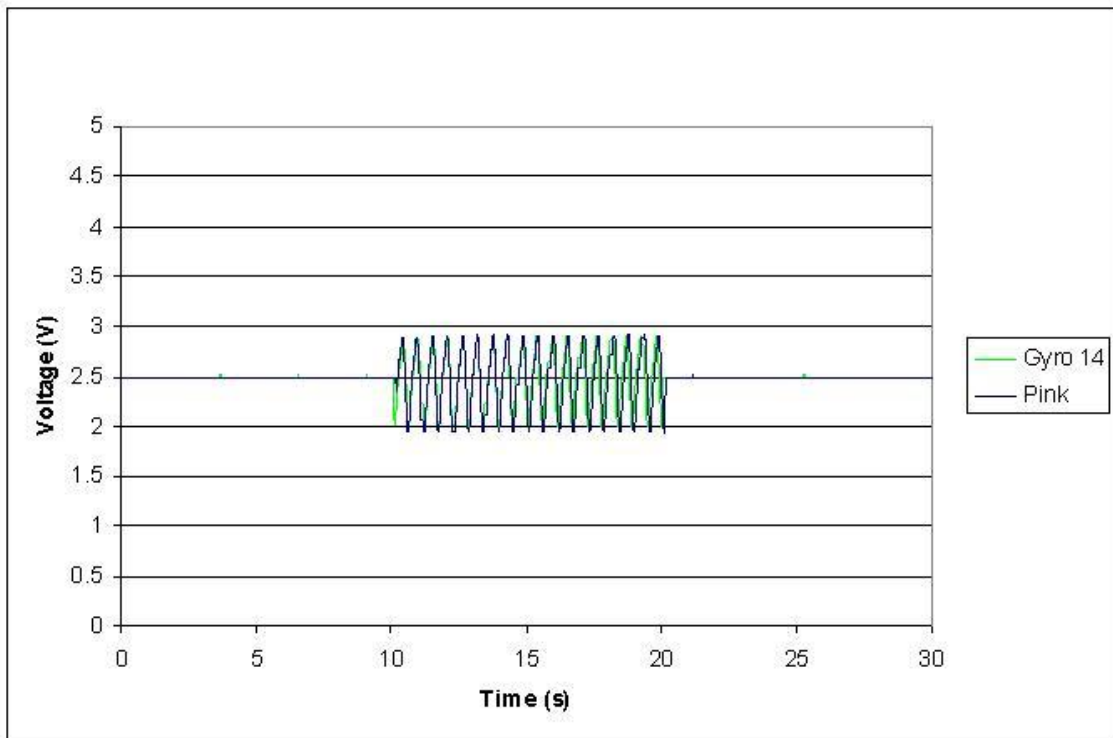


Figure 4.43: Output responses from gyro 14 without foam and with pink foam

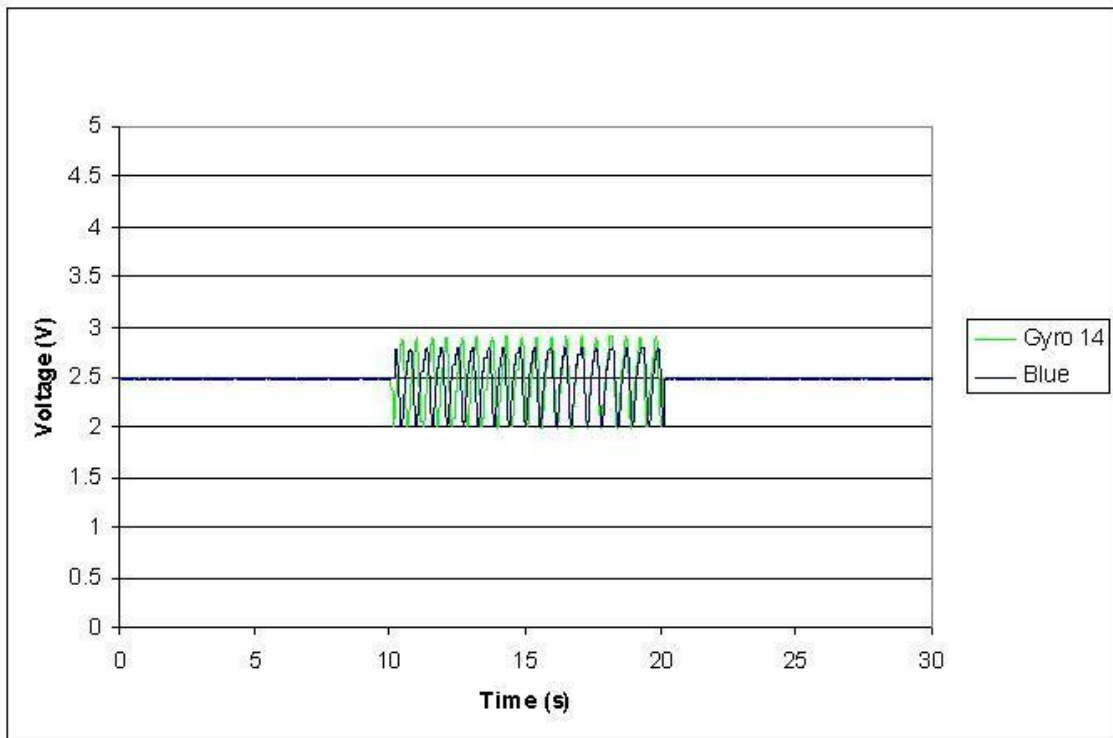


Figure 4.44: Output responses from gyro 14 without foam and with blue foam

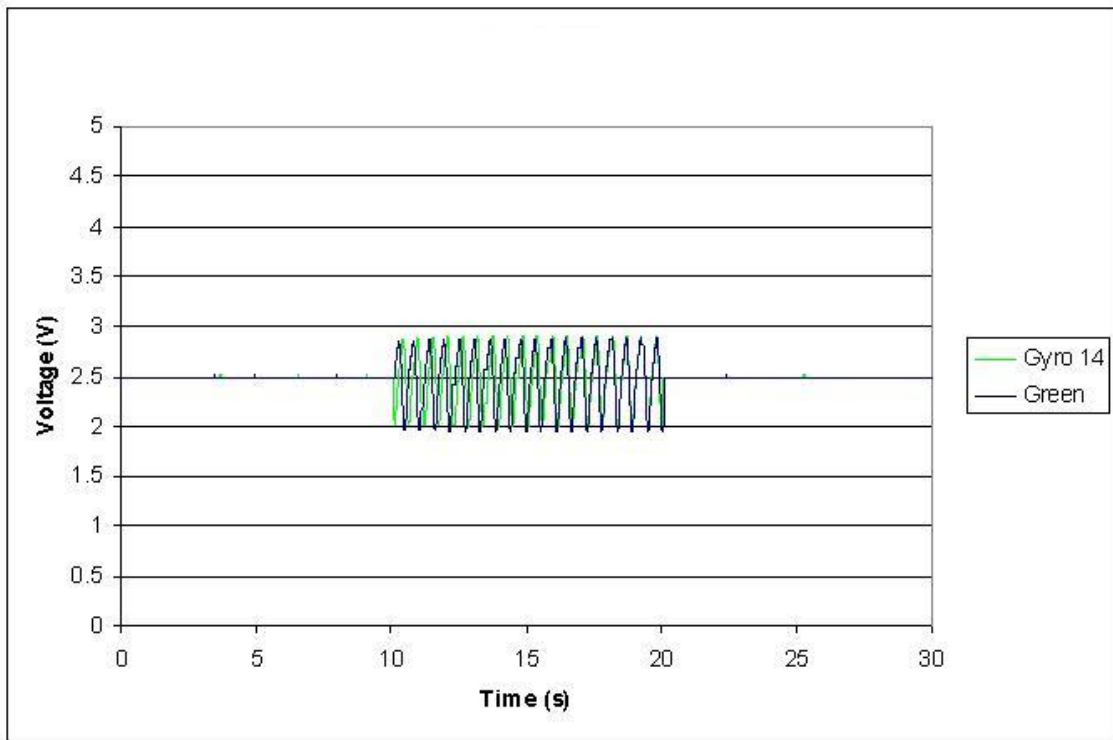


Figure 4.45: Output responses from gyro 14 without foam and with green foam

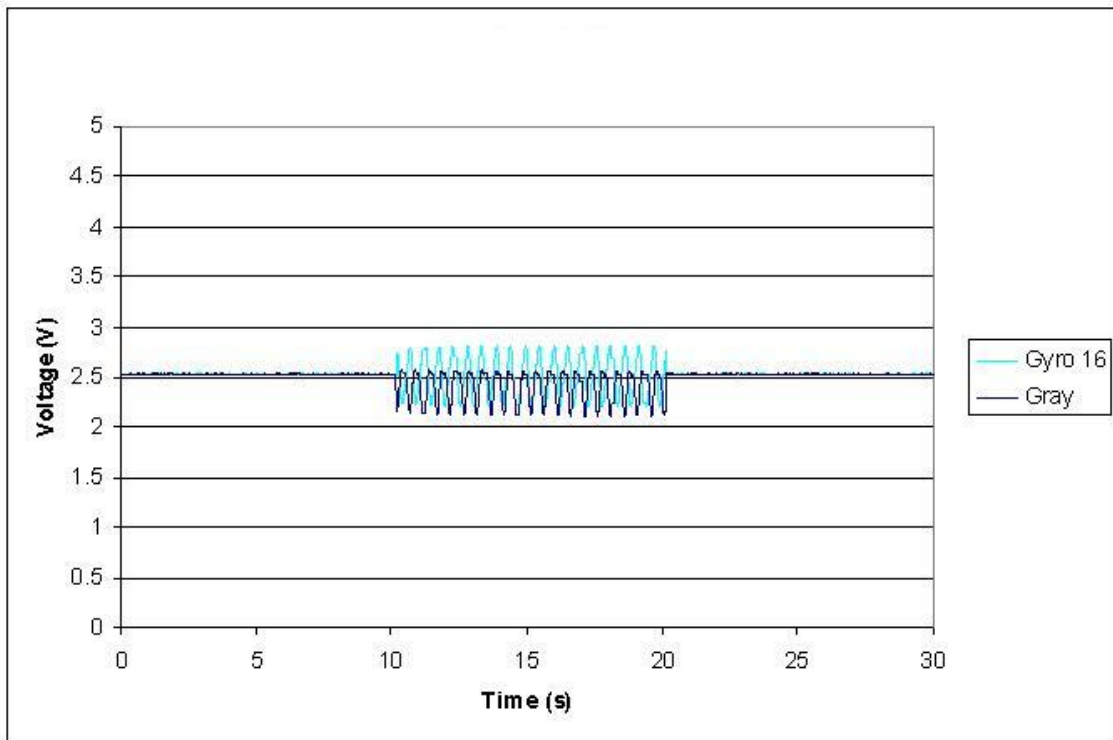


Figure 4.46: Output responses from gyro 16 without foam and with gray foam

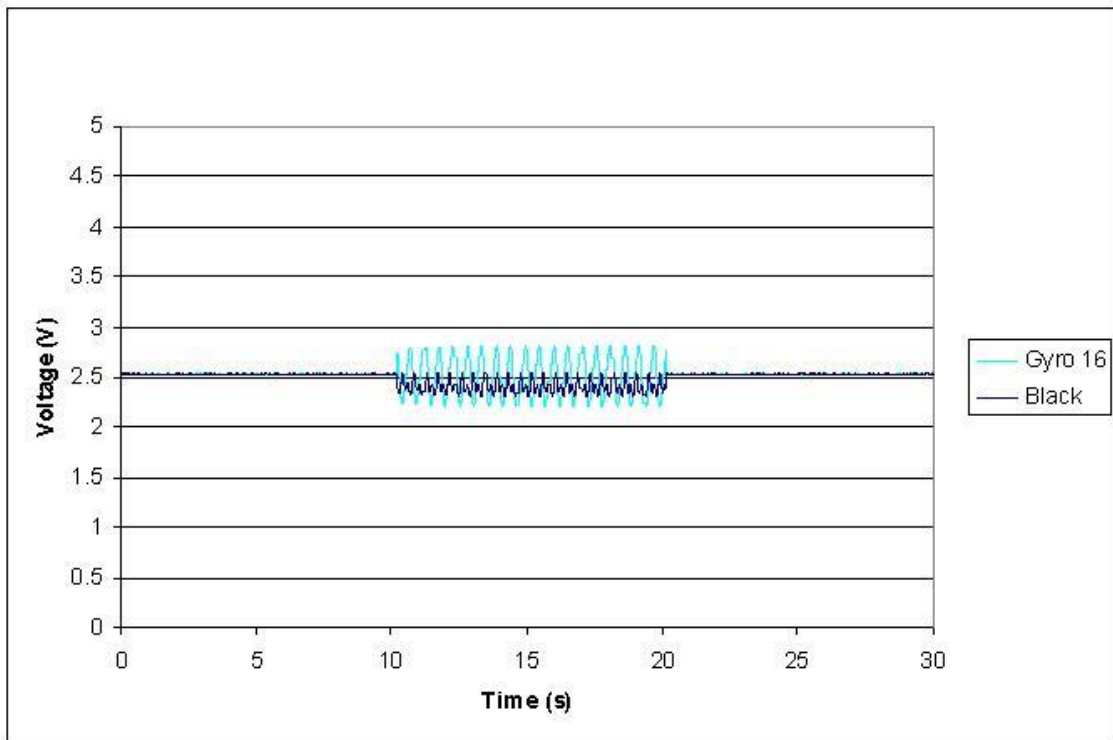


Figure 4.47: Output responses from gyro 16 without foam and with black foam

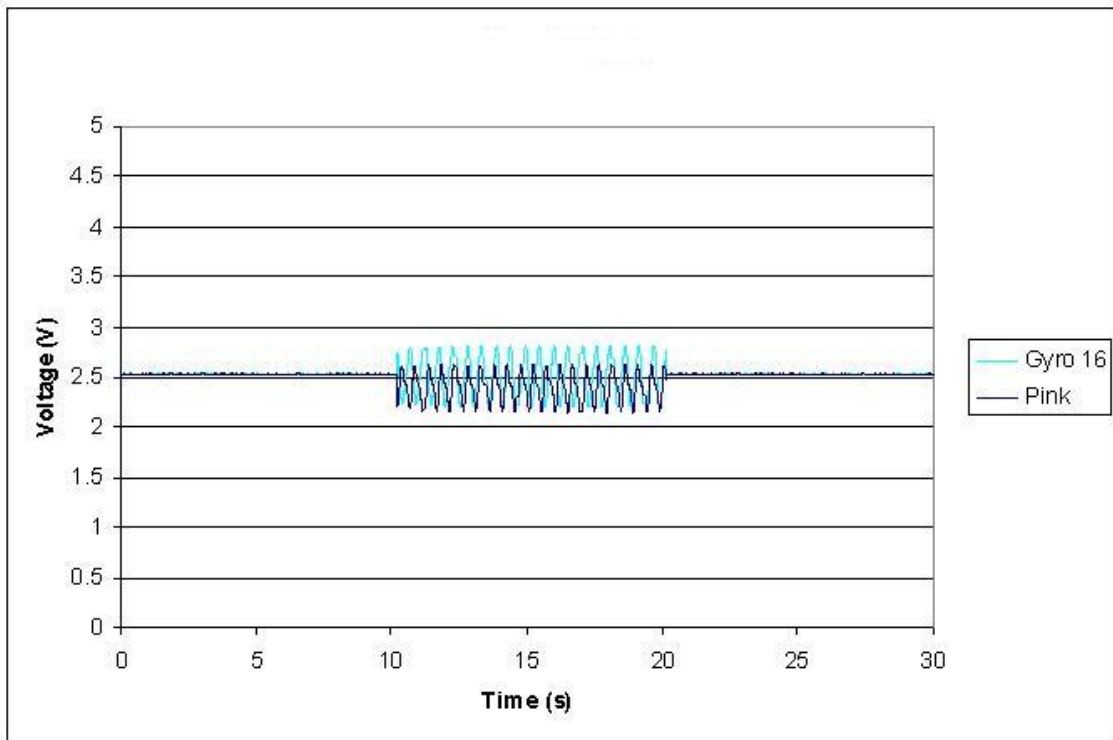


Figure 4.48: Output responses from gyro 16 without foam and with pink foam

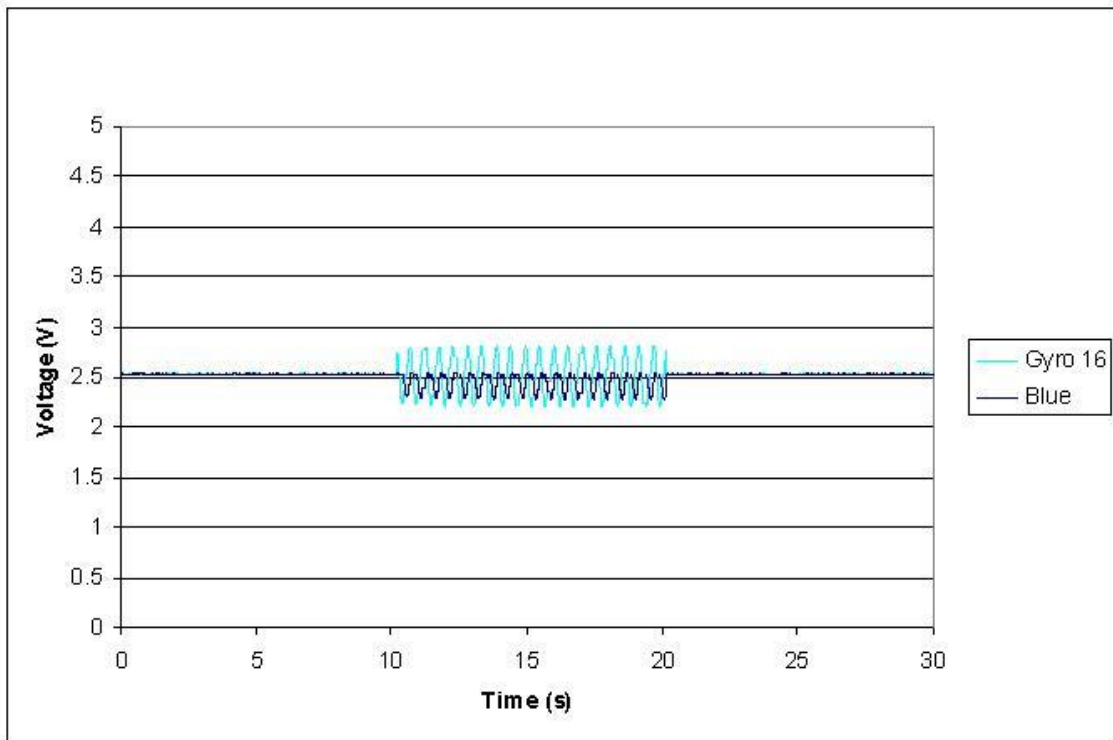


Figure 4.49: Output responses from gyro 16 without foam and with blue foam

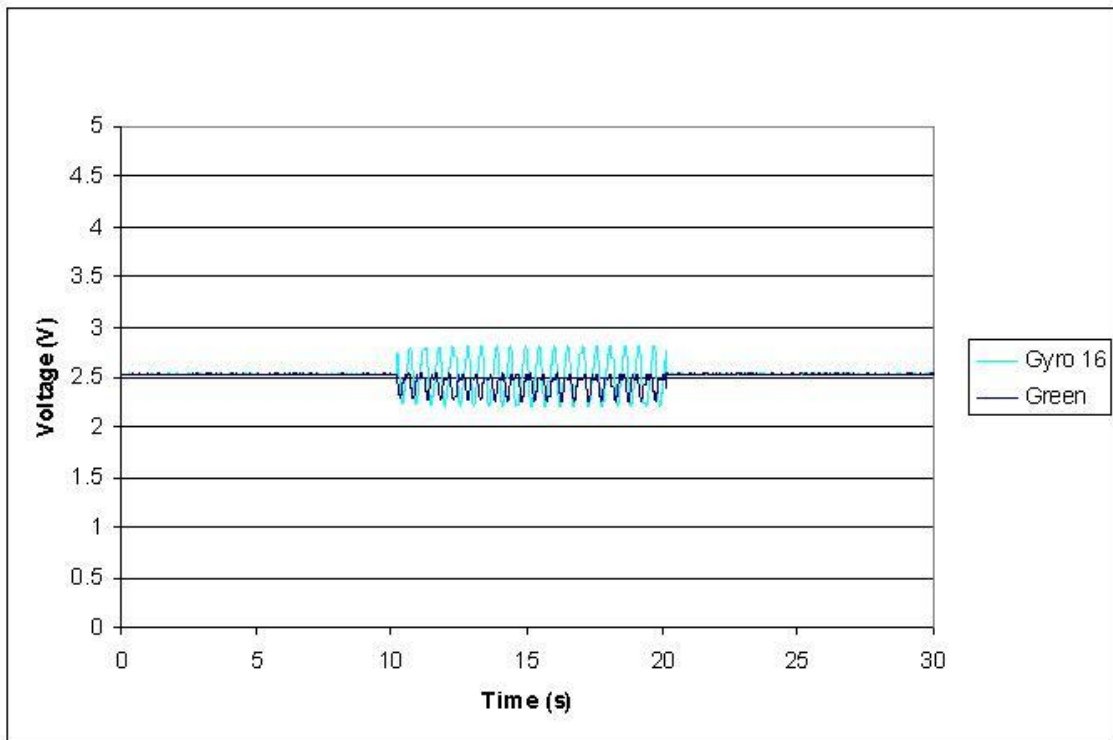


Figure 4.50: Output responses from gyro 16 without foam and with green foam

CHAPTER 5

CONCLUSION

Applications for MEMS gyroscopes have increased in recent years due to the small size and low cost of MEMS fabrication. Many of these environments include harsh conditions such as extreme temperatures, mechanical shock, vibration, and high frequency, high power acoustic noise. Studies have been performed by Weinberg on basic design error sources and by Pryputniewicz on the effects of temperatures on the packaging and devices. Studies have been performed by Dean, et. al., on the effects of vibrations and the means of isolation through the use of lowpass filters controlled with electrostatic actuation and signal processing [7] and by the use of mechanical filters made of either silicon or a polymer membrane[6]. The focus of this thesis was to demonstrate that MEMS Gyroscopes are susceptible to high power, high frequency acoustic noise and to evaluate ways of mitigating these effects.

The main task accomplished in this work was the creation of a model to simulate the effects of high frequency acoustic noise on a MEMS Gyroscope. The model was created using the base equations of motion of a vibratory MEMS Gyroscope and introducing a vibration into the equations to simulate the effects that acoustic noise would have on the gyroscope. This model was used to determine what type and amount of isolation were required to mitigate the adverse effects on the gyroscope's rate output due to acoustic noise. This data was then used to find similar foams with characteristics that corresponded to the simulated isolation. Experimental testing began without isolation to determine the effects on each of the gyroscopes that were used during the testing. These experiments demonstrated that there is

a wide range of effects that this noise can have on gyroscopes. After investigation, foams were found with characteristics similar to those used in the simulation. Tests were run with these foams in order to determine the ability of each foam to mitigate the effects of the acoustic noise. It was found that the denser black foam provided the best isolation from acoustic noise. The results from the gyro isolation tests also corresponded to the performed insertion loss tests. During the experimental testing several of the gyroscopes became unresponsive or intermittently responsive this could be due to prolonged exposure to the acoustic noise and warrants further investigation.

While the mitigation techniques used in this work only used several different types of foams, the study has provided a good background for work into the isolation of MEMS devices from high frequency, high power acoustic noise. This study provided a few means of mitigation of high frequency acoustic noise, the area remains open for further research into the field of mitigation techniques for acoustic noise isolation of MEMS devices.

BIBLIOGRAPHY

- [1] Gad-el-Hak, Mohamed, ed., *The MEMS Handbook*, CRC Press 2001.
- [2] Weinberg, Marc S.; Kourepenis, Anthony, "Error Sources in In-Plane Silicon Tuning Fork MEMS Gyroscopes," *Journal of Microelectromechanical Systems*, vol. 15, no. 3, June 2006, p 479-491.
- [3] Pryputniewicz, R J.; Marinis, Thomas F.; Soucy, Joseph W.; Furlong, Cosme, "Development of Packaging for MEMS Inertial Sensors," *Record - IEEE PLANS, Position Location and Navigation Symposium, PLANS - 2004 Position Location and Navigation Symposium*, 2004, p 56-62.
- [4] Dean, Robert N. ; Flowers, George T.; Hodel, A. Scotte; Roth, Grant; Castro, Simon; Zhou, Ran; Moreira, Alfonso; Ahmed, Anwar; Rifki, Rifki; Grantham, Brian E.; Bittle, David; Brunsch, J, "On the degradation of MEMS gyroscope performance in the presence of high power acoustic noise," *IEEE International Symposium on Industrial Electronics, 2007 IEEE International Symposium on Industrial Electronics, ISIE 2007, Proceedings*, 2007, p 1435-1440.
- [5] Castro, Simon; Roth, Grant; Dean, Robert; Flowers, George T.; Grantham, Brian, "Influence of acoustic noise on the dynamic performance of MEMS gyroscopes," *ASME International Mechanical Engineering Congress and Exposition, Proceedings*, v 9 PART C, *Proceedings of the ASME International Mechanical Engineering Congress and Exposition, IMECE 2007*, 2008, p 1825-1831.
- [6] Dean, Robert ; Flowers, George; Hodel, Scotte; MacAllister, Ken; Horvath, Roland; Matras, Alex; Glover, Rob, "Vibration isolation of MEMS sensors for aerospace applications," *Proceedings of SPIE - The International Society for Optical Engineering*, v 4828, 2002, p 166-170.
- [7] Dean, Robert; Flowers, George; Sanders, Nicole; MacAllister, Ken; Horvath, Roland; Hodel, A. Scotteward; Johnson, Wayne; Kranz, Michael; Whitley, Michael, "Damping control of micromachined lowpass mechanical vibration isolation filters using electrostatic actuation with electronic signal processing," *Proceedings of SPIE - The International Society for Optical Engineering*, v 5760, *Smart Structures and Materials 2005 - Damping and Isolation*, 2005, p 11-22.

- [8] Franden, Jacob, *AIP Handbook of Modern Sensors Physics, Designs and Applications* American Institute of Physics, 1993.
- [9] Beeby, Stephen; Ensell, Graham; Kraft, Michael; White, Neil, *MEMS Mechanical Sensors*, Artech House, Inc., 2004.
- [10] Kovacas, Gregory T.A., *Micromachined Transducers Sourcebook*, McGraw-Hill, 1998.
- [11] Patil, Nishad, "Design and Analysis of MEMS Angular Rate Sensors," *Master's Thesis*, Indian Institute of Science Bangalore, 2006.
- [12] Harris, Cyril M., *Handbook of Noise Control*, McGraw-Hill, 1957.
- [13] Saukoski, Mikko; Aaltonen, Lasse; Halonen, Kari A. I., "Zero-Rate Output and Quadrature Compensation in Vibratory MEMS Gyroscopes," *IEEE Sensors Journal*, v 7, no. 12, December 2007, p 1639-1652.

APPENDICES

APPENDIX A

DERIVATION OF EQUATIONS OF MOTION

The derivation of the Equations of Motion for a vibratory gyroscope using Lagrange's Equation. First find the kinetic energy

$$T = \frac{1}{2}m(\vec{V}_g \cdot \vec{V}_g) + \frac{1}{2}\vec{\omega} \cdot \vec{H}_g \quad (\text{A.1})$$

Given the following statements:

$$\vec{r}_o = x\hat{i} + y\hat{j} \quad (\text{A.2})$$

$$\vec{V}_o = \dot{x}\hat{i} + \dot{y}\hat{j} \quad (\text{A.3})$$

$$\vec{\omega} = \dot{\Theta}\hat{k} \quad (\text{A.4})$$

$$\vec{V}_g = \vec{V}_o + \vec{\omega} \times \vec{r}_o \quad (\text{A.5})$$

$$\vec{H}_g = \frac{1}{12}m(l_x^2 + l_y^2)\dot{\Theta} \quad (\text{A.6})$$

This leaves us with:

$$T = \frac{1}{2}m(\dot{x}^2 + \dot{y}^2 - 2\dot{\Theta}y\dot{x} + 2\dot{\Theta}x\dot{y} + \dot{\Theta}^2x^2 + \dot{\Theta}^2y^2) + \frac{1}{2}\left(\frac{1}{12}m(l_x^2 + l_y^2)\right)\dot{\Theta}^2 \quad (\text{A.7})$$

Next the *Rayleigh dissipation function* D and the potential energy:

$$D = \frac{1}{2}c_x\dot{x}^2 + \frac{1}{2}c_y\dot{y}^2 \quad (\text{A.8})$$

$$V = \frac{1}{2}k_x x^2 + \frac{1}{2}k_y y^2 \quad (\text{A.9})$$

Then find the Lagrange equations of motion by plugging A.7, A.8, and A.9 into:

$$\frac{d}{dt} \left(\frac{\partial T}{\partial \dot{q}_i} \right) - \frac{\partial T}{\partial q_i} + \frac{\partial D}{\partial \dot{q}_i} + \frac{\partial V}{\partial q_i} = Q_i \quad (\text{A.10})$$

Where i is x, y, Θ and

$$Q_x = F_d, Q_y = 0, Q_\Theta = 0$$

The equations of motion are:

$$m\ddot{x} + c_x \dot{x} + (k_x - m\dot{\Theta}^2)x - 2m\dot{\Theta}\dot{y} - m\ddot{\Theta}y = F_d \quad (\text{A.11})$$

$$m\ddot{y} + c_y \dot{y} + (k_y - m\dot{\Theta}^2)y + 2m\dot{\Theta}\dot{x} + m\ddot{\Theta}x = 0 \quad (\text{A.12})$$

$$m\ddot{\Theta}(x^2 + y^2 + \frac{1}{12}(l_x^2 + l_y^2)) + 2m\dot{\Theta}(x\dot{x} + y\dot{y}) - m\dot{y}\ddot{x} + m\dot{x}\ddot{y} = 0 \quad (\text{A.13})$$

APPENDIX B
SIMULATION CODE

B.1 Plotting

```
% This program is designed to plot a
% simulation of a 30 second test run
% of the gyroscopes in the acoustic chamber
% while not in motion
% It is divided into 3 phases
%*****
%Phase 1 Ten seconds of Silence
%*****
tic
clc
clear
delete *.mat
run('sim_run')
clear
run('init_Data')
format long

int=Tfinal-Timeglobal;
n=Timeglobal/Tstep;
Time1=Timeglobal;
```

```

if n==0;
    N=1;
else
    N=n;
end
nfinal=(Tfinal)/Tstep;

fileinit=int2str(N);
load (fileinit, 't','z')
i=1;
X=z(1,1);
X_dot=z(1,4);
Y=z(1,2);
Y_dot=z(1,5);
Theta=z(1,3);
Theta_dot=z(1,6);
for i=N:nfinal;

    file=int2str(i);
    load ( file, 't','z')
    ttemp=t;
    x=z(:,1);
    x_dot=z(:,4);
    y=z(:,2);
    y_dot=z(:,5);
    theta=z(:,3);
    theta_dot=z(:,6);
    clear t z

```

```

    Time1 = cat(1,Time1,ttemp);
    X_dot=cat(1,X_dot,x_dot);
    X=cat(1,X,x);
    Y_dot=cat(1,Y_dot,y_dot);
    Y=cat(1,Y,y);
    Theta_dot=cat(1,Theta_dot,theta_dot);
    Theta=cat(1,Theta,theta);
    i=i+1;

end

index_Time=length(Time1);
index=length(Theta_dot);

if index_Time==index
voltage_out1 = .0075*(180/pi*Theta_dot)+2.5;
end

save('phase1','Time1','voltage_out1')
%*****
%Phase 2 Ten seconds of Noise
%*****
run('sim_run2')
clear
run('init_Data2')
format long

int=Tfinal-Timeglobal;
n=Timeglobal/Tstep;
Time2=Timeglobal;

```



```

if n==0;
    N=1;
else
    N=n;
end
nfinal=(Tfinal)/Tstep;

fileinit=int2str(N);
load (fileinit, 't','z')
i=1;
X=z(1,1);
X_dot=z(1,4);
Y=z(1,2);
Y_dot=z(1,5);
Theta=z(1,3);
Theta_dot=z(1,6);
for i=N:nfinal;

    file=int2str(i);
    load ( file, 't','z')
    ttemp=t;
    x=z(:,1);
    x_dot=z(:,4);
    y=z(:,2);
    y_dot=z(:,5);
    theta=z(:,3);
    theta_dot=z(:,6);
    clear t z
    Time2 = cat(1,Time2,ttemp);

```

```

X_dot=cat(1,X_dot,x_dot);
X=cat(1,X,x);
Y_dot=cat(1,Y_dot,y_dot);
Y=cat(1,Y,y);
Theta_dot=cat(1,Theta_dot,theta_dot);
Theta=cat(1,Theta,theta);
i=i+1;

end

index_Time=length(Time2);
index=length(Theta_dot);

if index_Time==index
voltage_out2 = .0075*(180/pi*Theta_dot)+2.5;
end

save('phase2','Time2','voltage_out2')

%*****
%Phase 3 Ten seconds of silence
%*****

run('sim_run3')
clear
run('init_Data3')
format long

int=Tfinal-Timeglobal;
n=Timeglobal/Tstep;
Time3=Timeglobal;

```

```

if n==0;
    N=1;
else
    N=n;
end
nfinal=(Tfinal)/Tstep;

fileinit=int2str(N);
load (fileinit, 't','z')
i=1;
X=z(1,1);
X_dot=z(1,4);
Y=z(1,2);
Y_dot=z(1,5);
Theta=z(1,3);
Theta_dot=z(1,6);
for i=N:nfinal;

    file=int2str(i);
    load ( file, 't','z')
    ttemp=t;
    x=z(:,1);
    x_dot=z(:,4);
    y=z(:,2);
    y_dot=z(:,5);
    theta=z(:,3);
    theta_dot=z(:,6);
    clear t z
    Time3 = cat(1,Time3,ttemp);

```

```

X_dot=cat(1,X_dot,x_dot);
X=cat(1,X,x);
Y_dot=cat(1,Y_dot,y_dot);
Y=cat(1,Y,y);
Theta_dot=cat(1,Theta_dot,theta_dot);
Theta=cat(1,Theta,theta);
i=i+1;

end

index_Time=length(Time3);
index=length(Theta_dot);

if index_Time==index
voltage_out3 = .0075*(180/pi*Theta_dot)+2.5;
end
load('phase1','Time1','voltage_out1')
load('phase2','Time2','voltage_out2')

Tot_Time = decimate(cat(1,Time1,Time2,Time3),decval);
Tot_voltage=decimate(cat(1,voltage_out1,voltage_out2,voltage_out3),
                    decval);
plot(Tot_Time,Tot_voltage),title('Voltage Output vs Time'),
     xlabel('Time (s)'),ylabel('Voltage Out (V)'),ylim([0,5])

RunTime = toc

save('good/no.noise','Tot_Time','Tot_voltage')

```

B.2 Initialization Data

B.2.1 init_Data.m

```
eo=8.854e-12;
er=1.00054;
V0=12; %Voltage from charge pump
Vac=6; %AC drive voltage
num=2500; %Number of comb fingers on
thick=4e-6;%Thickness of gyro structure
widthleg=1.7e-6;%Width of legs
m=8e-9; %Mass of Proof mass
driveamp=7e-6;%amplitude of drive
V.bias= 12; %Volts
Vn=10e-8;
CapSum=12e-12;
Capc=1e-13;
Vc=.2;
g=1.7e-6;
phase_shift=0;
lc=1.7e-6;%50e-6;
x0=7e-6;%amplitude of drive
alpha=1e-6;
l1=1e-3;
l2=5e-4;
fn=14000; %rate ADXRS300 proofmass is supposed to vibrate

ratio= 1.2;%the ratio between drive and sense usually sense is
           %approximately 20% higher than drive
Q=45;%QUALITY FACTOR
```

```

diffchange=2e-12/3e-6;
feedback =2e-12;

%Frequencies and Spring Rates
wn1= 2*pi*fn;
wn2= 2*pi*fn*ratio;
k1= wn1*wn1*m;
k2= wn2*wn2*m;

c1= m*wn1/Q;
c2= m*wn2/Q;

decval = 200;

%Rotational Rate Information
rotationDegrees=0; % Initial Rotational Rate of the Gyroscope
omega_in=rotationDegrees*(pi/180);
%Acoustic Noise Parameters
noiseamount=0; %sound level in dB
noisefreq=0;
%noise_isolation=0;

Tstep=.1;
Timeglobal= 0;
Tfinal=10;

```

B.2.2 init_Data2.m

```
run('init_Data')  
  
%Acoustic Noise Parameters  
soundlevel=30;%sound level in dB minus 100  
noise_isolation=0;%reduction in dB  
noiseamount=(soundlevel-noise_isolation)*.75;  
noisefreq=wn2;  
  
Timeglobal= 10;  
Tfinal=20;
```

B.2.3 init_Data3.m

```
run('init_Data')
```

```
Timeglobal= 20;
```

```
Tfinal=30;
```


B.3 Files That Run ode45

B.3.1 sim_run.m

```
clc
clear all

close all

run('init_Data');

x0=0;
xd0=0;
xdd0=0;
y0=0;
yd0=0;
ydd0=0;
theta0=0;
thetad0=omega_in;
thetadd0=0;

z0=[x0,y0,theta0,xd0,yd0,thetad0];

options = odeset('RelTol',1e-3,'InitialStep', 1e-16);
t=0;
int=Tfinal-Timeglobal;
n=Timeglobal/Tstep;
Time=Timeglobal;
if n==0;
```

```

    N=1;
else N=n;
    fileinitial = int2str(N);
    load(fileinitial, 'z');
    Lin=size(z);
    xinit=z(Lin(1),1);
    yinit=z(Lin(1),2);
    thetainit=z(Lin(1),3);
    xdinit=z(Lin(1),4);
    ydinit=z(Lin(1),5);
    thetadinit=z(Lin(1),6);
    clear z
end
n=n+1;
while Timeglobal<Tfinal;
    if Timeglobal==0;
        zinitcond=z0;
        timestep=Tstep;
    else
        zinitcond=[xinit,yinit,thetainit,xdinit,ydinit,thetadinit];
        time=Timeglobal;
    end
    timestep=Tstep+Timeglobal;

    [t,z]=ode45(@sim-try,[Timeglobal timestep],zinitcond,options);

    filename=int2str(n);
    save(filename, 't', 'z')
    clear t z;
    load(filename, 't', 'z')

```

```
L=size(z);
xinit=z(L(1),1);
yinit=z(L(1),2);
thetainit=z(L(1),3);
xdinit=z(L(1),4);
ydinit=z(L(1),5);
thetadinit=z(L(1),6);
clear t z;

Timeglobal=Timeglobal+Tstep;
n=n+1;
end
```

B.3.2 sim_run2.m

```
clc
clear all

close all

run('init_Data2');

x0=0;
xd0=0;
xdd0=0;
y0=0;
yd0=0;
ydd0=0;
theta0=0;
thetad0=omega_in;
thetadd0=0;

z0=[x0,y0,theta0,xd0,yd0,thetad0];

options = odeset('RelTol',1e-3,'InitialStep', 1e-16);
t=0;
int=Tfinal-Timeglobal;
n=Timeglobal/Tstep;
Time=Timeglobal;
if n==0;
    N=1;
else N=n+1;
```

```

file = int2str(n);
load(file, 'z')
Lin=size(z);
xinit=z(Lin(1),1);
yinit=z(Lin(1),2);
thetainit=z(Lin(1),3);
xdinit=z(Lin(1),4);
ydinit=z(Lin(1),5);
thetadinit=z(Lin(1),6);
clear z
end
n=n+1;
while Timeglobal<Tfinal;
    if Timeglobal==0;
        zinitcond=z0;
        timestep=Tstep;
    else
        zinitcond=[xinit,yinit,thetainit,xdinit,ydinit,thetadinit];
        time=Timeglobal;
    end
    timestep=Tstep+Timeglobal;

    [t,z]=ode45(@sim_try2,[Timeglobal timestep],zinitcond,options);

    filename=int2str(n);
    save(filename, 't', 'z')
    clear t z;
    load(filename, 't', 'z')

    L=size(z);
    xinit=z(L(1),1);

```

```
yinit=z(L(1),2);  
thetainit=z(L(1),3);  
xdinit=z(L(1),4);  
ydinit=z(L(1),5);  
thetadinit=z(L(1),6);  
clear t z;  
  
Timeglobal=Timeglobal+Tstep;  
n=n+1;  
end
```

B.3.3 sim_run3.m

```
clc
clear all

close all

run('init_Data3');

x0=0;
xd0=0;
xdd0=0;
y0=0;
yd0=0;
ydd0=0;
theta0=0;
thetad0=omega_in;
thetadd0=0;

z0=[x0,y0,theta0,xd0,yd0,thetad0];

options = odeset('RelTol',1e-3,'InitialStep', 1e-16);
t=0;
int=Tfinal-Timeglobal;
n=Timeglobal/Tstep;
Time=Timeglobal;
if n==0;
    N=1;
else N=n;
```

```

file = int2str(n);
load(file, 'z');
Lin=size(z);
xinit=z(Lin(1),1);
yinit=z(Lin(1),2);
thetainit=z(Lin(1),3);
xdinit=z(Lin(1),4);
ydinit=z(Lin(1),5);
thetadinit=z(Lin(1),6);
clear z
end
n=n+1;
while Timeglobal<Tfinal;
    if Timeglobal==0;
        zinitcond=z0;
        timestep=Tstep;
    else
        zinitcond=[xinit,yinit,thetainit,xdinit,ydinit,thetadinit];
        time=Timeglobal;
    end
    timestep=Tstep+Timeglobal;

    [t,z]=ode45(@sim_try3,[Timeglobal timestep],zinitcond,options);

    filename=int2str(n);
    save(filename, 't', 'z')
    clear t z;
    load(filename, 't', 'z')

    L=size(z);
    xinit=z(L(1),1);

```



```
yinit=z(L(1),2);  
thetainit=z(L(1),3);  
xdinit=z(L(1),4);  
ydinit=z(L(1),5);  
thetadinit=z(L(1),6);  
  
clear t z;  
  
Timeglobal=Timeglobal+Tstep;  
n=n+1;  
end
```

B.4 Equations of Motion

B.4.1 sim_try.m

```
function zprime=sim_try(t,z)
run('init_Data')
xd= sin(wn1*t);
Fx=(2.28*num*eo*thick*V0*Vac*xd)/g;
noise=noiseamount*sin((noisefreq)*t);

x=z(1);
y=z(2);
theta=z(3);
xdot=z(4);
ydot=z(5);
thetadot=z(6);

%Linearized equations
xprime=xdot;
yprime=ydot;
thetaprime=thetadot;

xdotprime =(12*Fx*m*x^2+x*k1*l2^2-12*x^3*k1*m+x*k1*l1^2+12*x*k1*y^2
-12*x^3*m*thetadot^2+c1*xdot*l2^2+12*c1*xdot*x^2
+24*noise*m*x^2+12*c1*xdot*y^2+c1*xdot*l1^2
+12*x^3*m^2*thetadot^2-12*c1*xdot*m*x^2
+12*x*m^2*thetadot^2*y^2-x*m*thetadot^2*l1^2
-x*m*thetadot^2*l2^2-12*x*m*thetadot^2*y^2
-2*m*thetadot*ydot*l1^2+24*m^2*thetadot*ydot*x^2
```

$$\begin{aligned}
& -2*m*\text{thetadot}*y\text{dot}*l2^2-24*m*\text{thetadot}*y\text{dot}*x^2 \\
& +12*m*y*x*\text{noise}-12*m*y^2*x*k2-Fx*l1^2 \\
& -Fx*l2^2-12*Fx*x^2-12*Fx*y^2-2*\text{noise}*l1^2-2*\text{noise}*l2^2 \\
& -24*\text{noise}*x^2-24*\text{noise}*y^2+12*x^3*k1+24*m*y*\text{thetadot}*x*\text{xdot} \\
& -24*m^2*y*x*\text{thetadot}*x\text{dot}-12*m*y*x*c2*y\text{dot}) / (12*m*y^2-l1^2 \\
& +12*m*x^2-l2^2-12*x^2-12*y^2);
\end{aligned}$$

$$\begin{aligned}
y\text{dotprime} = & (12*y*k2*x^2+12*c2*y\text{dot}*y^2-12*y^3*k2*m+y*k2*l1^2 \\
& -12*y^3*m*\text{thetadot}^2+y*k2*l2^2+12*c2*y\text{dot}*x^2+c2*y\text{dot}*l1^2 \\
& +c2*y\text{dot}*l2^2+12*y^3*m^2*\text{thetadot}^2+12*\text{noise}*m*y^2 \\
& +24*m*y*x*\text{noise}-12*c2*y\text{dot}*m*y^2-y*m*\text{thetadot}^2*l1^2 \\
& +12*y*m^2*\text{thetadot}^2*x^2-y*m*\text{thetadot}^2*l2^2 \\
& -12*y*m*\text{thetadot}^2*x^2-24*m^2*\text{thetadot}*x\text{dot}*y^2 \\
& +2*m*\text{thetadot}*x\text{dot}*l1^2+2*m*\text{thetadot}*x\text{dot}*l2^2 \\
& +24*m*\text{thetadot}*x\text{dot}*y^2-\text{noise}*l1^2 \\
& -\text{noise}*l2^2-12*\text{noise}*x^2-12*\text{noise}*y^2+12*y^3*k2+12*m*x*y*Fx \\
& -12*m*x^2*y*k1-24*m*x*\text{thetadot}*y*y\text{dot} \\
& +24*m^2*x*y*\text{thetadot}*y\text{dot}-12*m*x*y*c1*x\text{dot}) \\
& / (12*m*y^2-l1^2+12*m*x^2-l2^2-12*x^2-12*y^2);
\end{aligned}$$

$$\begin{aligned}
\text{thetadotprime} = & 12*(-y*Fx+x*\text{noise}+2*\text{thetadot}*x*\text{xdot}+2*\text{thetadot}*y*y\text{dot} \\
& -2*y*m*\text{thetadot}*y\text{dot}-2*y*\text{noise}+y*c1*x\text{dot}+y*x*k1 \\
& -2*x*m*\text{thetadot}*x\text{dot}-x*c2*y\text{dot}-x*y*k2) / (12*m*y^2-l1^2 \\
& +12*m*x^2-l2^2-12*x^2-12*y^2);
\end{aligned}$$

$$z\text{prime}(1) = x\text{prime};$$

$$z\text{prime}(2) = y\text{prime};$$

$$z\text{prime}(3) = \text{thetaprime};$$

$$z\text{prime}(4) = x\text{dotprime};$$

$$z\text{prime}(5) = y\text{dotprime};$$

$$z\text{prime}(6) = \text{thetadotprime};$$

```
zprime=zprime';
```

B.4.2 sim_try2.m

```
function zprime=sim_try2(t,z)
run('init_Data2')
xd= sin(wn1*t);
Fx=(2.28*num*eo*thick*V0*Vac*xd)/g;
noise=noiseamount*sin((noisefreq)*t);

x=z(1);
y=z(2);
theta=z(3);
xdot=z(4);
ydot=z(5);
thetadot=z(6);

%Linearized equations
xprime=xdot;
yprime=ydot;
thetaprime=thetadot;

xdotprime =(12*Fx*m*x^2+x*k1*l2^2-12*x^3*k1*m+x*k1*l1^2+12*x*k1*y^2
-12*x^3*m*thetadot^2+c1*xdot*l2^2+12*c1*xdot*x^2
+24*noise*m*x^2+12*c1*xdot*y^2+c1*xdot*l1^2
+12*x^3*m^2*thetadot^2-12*c1*xdot*m*x^2
+12*x*m^2*thetadot^2*y^2-x*m*thetadot^2*l1^2
-x*m*thetadot^2*l2^2-12*x*m*thetadot^2*y^2
-2*m*thetadot*ydot*l1^2+24*m^2*thetadot*ydot*x^2
-2*m*thetadot*ydot*l2^2-24*m*thetadot*ydot*x^2
+12*m*y*x*noise-12*m*y^2*x*k2-Fx*l1^2
```

$$\begin{aligned}
& -Fx*12^2-12*Fx*x^2-12*Fx*y^2-2*noise*11^2-2*noise*12^2 \\
& -24*noise*x^2-24*noise*y^2+12*x^3*k1+24*m*y*thetadot*x*xdot \\
& -24*m^2*y*x*thetadot*xdot-12*m*y*x*c2*ydot) / (12*m*y^2-11^2 \\
& +12*m*x^2-12^2-12*x^2-12*y^2);
\end{aligned}$$

$$\begin{aligned}
ydotprime = & (12*y*k2*x^2+12*c2*ydot*y^2-12*y^3*k2*m+y*k2*11^2 \\
& -12*y^3*m*thetadot^2+y*k2*12^2+12*c2*ydot*x^2+c2*ydot*11^2 \\
& +c2*ydot*12^2+12*y^3*m^2*thetadot^2+12*noise*m*y^2 \\
& +24*m*y*x*noise-12*c2*ydot*m*y^2-y*m*thetadot^2*11^2 \\
& +12*y*m^2*thetadot^2*x^2-y*m*thetadot^2*12^2 \\
& -12*y*m*thetadot^2*x^2-24*m^2*thetadot*xdot*y^2 \\
& +2*m*thetadot*xdot*11^2+2*m*thetadot*xdot*12^2 \\
& +24*m*thetadot*xdot*y^2-noise*11^2 \\
& -noise*12^2-12*noise*x^2-12*noise*y^2+12*y^3*k2+12*m*x*y*Fx \\
& -12*m*x^2*y*k1-24*m*x*thetadot*y*ydot \\
& +24*m^2*x*y*thetadot*ydot-12*m*x*y*c1*xdot) \\
& / (12*m*y^2-11^2+12*m*x^2-12^2-12*x^2-12*y^2);
\end{aligned}$$

$$\begin{aligned}
thetadotprime = & 12*(-y*Fx+x*noise+2*thetadot*x*xdot+2*thetadot*y*ydot \\
& -2*y*m*thetadot*ydot-2*y*noise+y*c1*xdot+y*x*k1 \\
& -2*x*m*thetadot*xdot-x*c2*ydot-x*y*k2) / (12*m*y^2-11^2 \\
& +12*m*x^2-12^2-12*x^2-12*y^2);
\end{aligned}$$

```

zprime(1)=xprime;
zprime(2)=yprime;
zprime(3)=thetaprime;
zprime(4)=xdotprime;
zprime(5)=ydotprime;
zprime(6)=thetadotprime;
zprime=zprime';

```

B.4.3 sim_try3.m

```
function zprime=sim_try3(t,z)
run('init_Data3')
xd= sin(wn1*t);
Fx=(2.28*num*eo*thick*V0*Vac*xd)/g;
noise=noiseamount*sin((noisefreq)*t);

x=z(1);
y=z(2);
theta=z(3);
xdot=z(4);
ydot=z(5);
thetadot=z(6);

%Linearized equations
xprime=xdot;
yprime=ydot;
thetaprime=thetadot;

xdotprime =(12*Fx*m*x^2+x*k1*l2^2-12*x^3*k1*m+x*k1*l1^2+12*x*k1*y^2
-12*x^3*m*thetadot^2+c1*xdot*l2^2+12*c1*xdot*x^2
+24*noise*m*x^2+12*c1*xdot*y^2+c1*xdot*l1^2
+12*x^3*m^2*thetadot^2-12*c1*xdot*m*x^2
+12*x*m^2*thetadot^2*y^2-x*m*thetadot^2*l1^2
-x*m*thetadot^2*l2^2-12*x*m*thetadot^2*y^2
-2*m*thetadot*ydot*l1^2+24*m^2*thetadot*ydot*x^2
-2*m*thetadot*ydot*l2^2-24*m*thetadot*ydot*x^2
+12*m*y*x*noise-12*m*y^2*x*k2-Fx*l1^2
```

$$\begin{aligned}
& -Fx*12^2-12*Fx*x^2-12*Fx*y^2-2*noise*11^2-2*noise*12^2 \\
& -24*noise*x^2-24*noise*y^2+12*x^3*k1+24*m*y*thetadot*x*xdot \\
& -24*m^2*y*x*thetadot*xdot-12*m*y*x*c2*ydot) / (12*m*y^2-11^2 \\
& +12*m*x^2-12^2-12*x^2-12*y^2);
\end{aligned}$$

$$\begin{aligned}
ydotprime = & (12*y*k2*x^2+12*c2*ydot*y^2-12*y^3*k2*m+y*k2*11^2 \\
& -12*y^3*m*thetadot^2+y*k2*12^2+12*c2*ydot*x^2+c2*ydot*11^2 \\
& +c2*ydot*12^2+12*y^3*m^2*thetadot^2+12*noise*m*y^2 \\
& +24*m*y*x*noise-12*c2*ydot*m*y^2-y*m*thetadot^2*11^2 \\
& +12*y*m^2*thetadot^2*x^2-y*m*thetadot^2*12^2 \\
& -12*y*m*thetadot^2*x^2-24*m^2*thetadot*xdot*y^2 \\
& +2*m*thetadot*xdot*11^2+2*m*thetadot*xdot*12^2 \\
& +24*m*thetadot*xdot*y^2-noise*11^2 \\
& -noise*12^2-12*noise*x^2-12*noise*y^2+12*y^3*k2+12*m*x*y*Fx \\
& -12*m*x^2*y*k1-24*m*x*thetadot*y*ydot \\
& +24*m^2*x*y*thetadot*ydot-12*m*x*y*c1*xdot) \\
& / (12*m*y^2-11^2+12*m*x^2-12^2-12*x^2-12*y^2);
\end{aligned}$$

$$\begin{aligned}
thetadotprime = & 12*(-y*Fx+x*noise+2*thetadot*x*xdot+2*thetadot*y*ydot \\
& -2*y*m*thetadot*ydot-2*y*noise+y*c1*xdot+y*x*k1 \\
& -2*x*m*thetadot*xdot-x*c2*ydot-x*y*k2) / (12*m*y^2-11^2 \\
& +12*m*x^2-12^2-12*x^2-12*y^2);
\end{aligned}$$

```

zprime(1)=xprime;
zprime(2)=yprime;
zprime(3)=thetaprime;
zprime(4)=xdotprime;
zprime(5)=ydotprime;
zprime(6)=thetadotprime;
zprime=zprime';

```